

Rothamsted Repository Download

A - Papers appearing in refereed journals

Kroll, E., Bayon, C., Rudd, J. J., Armer, V., Magaji-Umashankar, A., Ames, R., Urban, M., Brown, N. A. and Hammond-Kosack, K. E. 2025. A conserved fungal Knr4/Smi1 protein is vital for maintaining cell wall integrity and host plant pathogenesis . *PLOS Pathogens*. 21 (1), p. e1012769. <https://doi.org/10.1371/journal.ppat.1012769>

The publisher's version can be accessed at:

- <https://doi.org/10.1371/journal.ppat.1012769>
- <https://www.biorxiv.org/content/10.1101/2024.05.31.596832v1>

The output can be accessed at: <https://repository.rothamsted.ac.uk/item/99072/a-conserved-fungal-knr4-smi1-protein-is-vital-for-maintaining-cell-wall-integrity-and-host-plant-pathogenesis>.

© 9 January 2025, Please contact library@rothamsted.ac.uk for copyright queries.

1 **A conserved fungal Knr4/Smi1 protein is vital**
2 **for maintaining cell wall integrity and host**
3 **plant pathogenesis**

4 **Erika Kroll^{1,2}, Carlos Bayon¹, Jason Rudd¹, Victoria Armer¹, Anjana Magaji-**
5 **Umashankar¹, Ryan Ames³, Martin Urban¹, Neil A. Brown², and Kim Hammond-**
6 **Kosack^{1,*}**

7 Author addresses: ¹Strategic Area: Protecting Crops and the Environment, Rothamsted
8 Research, Harpenden, AL5 2JQ, UK

9 ²Department of Life Sciences, University of Bath, Bath, BA2 7AY, UK

10 ³Biosciences and Living Systems Institute, University of Exeter, EX4 4PY, Exeter, UK

11 **Corresponding authors:**

12 *To whom correspondence should be addressed. Tel: +44 1582 938240. Email:

13 kim.hammond-kosack@rothamsted.ac.uk

14

15 **Abstract**

16 Filamentous plant pathogenic fungi pose significant threats to global food security,
17 particularly through diseases like Fusarium Head Blight (FHB) and Septoria Tritici Blotch
18 (STB) which affects cereals. With mounting challenges in fungal control and increasing
19 restrictions on fungicide use due to environmental concerns, there is an urgent need for
20 innovative control strategies. Here, we present a comprehensive analysis of the stage-
21 specific infection process of *Fusarium graminearum* in wheat spikes by generating a dual
22 weighted gene co-expression network (WGCN). Notably, the network contained a
23 mycotoxin-enriched fungal module that exhibited a significant correlation with a detoxification
24 gene-enriched wheat module. This correlation in gene expression was validated through
25 quantitative PCR.

26 By examining a fungal module with genes highly expressed during early symptomless
27 infection, we identified a gene encoding FgKnr4, a protein containing a Knr4/Smi1
28 disordered domain. Through comprehensive analysis, we confirmed the pivotal role of
29 FgKnr4 in various biological processes, including morphogenesis, growth, cell wall stress
30 tolerance, and pathogenicity. Further studies confirmed the observed phenotypes are
31 partially due to the involvement of FgKnr4 in regulating the fungal cell wall integrity pathway
32 by modulating the phosphorylation of the MAP-kinase MGV1. Orthologues of the *FgKnr4*
33 gene are widespread across the fungal kingdom but are absent in other Eukaryotes,
34 suggesting the protein has potential as a promising intervention target. Encouragingly, the
35 restricted growth and highly reduced virulence phenotypes observed for $\Delta Fgknr4$ were
36 replicated upon deletion of the orthologous gene in the wheat fungal pathogen *Zymoseptoria*
37 *tritici*. Overall, this study demonstrates the utility of an integrated network-level analytical
38 approach to pinpoint genes of high interest to pathogenesis and disease control.

39 **Keywords: *Fusarium graminearum*, *Zymoseptoria tritici*, Weighted Gene Co-**
40 **expression Network (WGCNA), dual host-pathogen transcriptomics, cell wall stress,**
41 **MAP-kinase signalling, fungal specific gene family, fungal virulence.**

42

43 **Introduction**

44 The wheat crop (*Triticum* species) plays a crucial role in global food security, contributing
45 about 20% of dietary calories and protein worldwide (Saldivar, 2016), while also supplying
46 essential nutrients and bioactive food components (Shewry and Hey, 2015). Pathogen and
47 pest burden substantially contribute to wheat losses globally, accounting for ~21.5% of
48 wheat losses annually (Savary et al., 2019). Of these, the five highest global contributors to
49 wheat yield and quality losses are all fungal diseases and include Fusarium Head Blight
50 disease (FHB) and Septoria tritici blotch disease (STB), which account for 2.85% and 2.44%
51 of wheat losses, respectively (Savary et al., 2019).

52 FHB is a mycotoxigenic pre-harvest fungal disease of most cereals, caused by different
53 *Fusaria* within the *Fusarium sambucinum* species complex that is increasingly prevalent in
54 most cereal growing regions globally (O'Donnell et al., 2000; Kanja et al., 2021; Johns et al.,
55 2022; Armer et al., 2024). Floral Infections lead to contamination of grain with mycotoxins
56 that are subject to strict legal limits in different global regions (European Commission, 2006;
57 EFSA, 2017; AHDB, 2023). Despite ongoing endeavours to manage FHB, mycotoxin
58 contamination continues to significantly impact the economies of cereal and livestock
59 producers, as well as the food, drink, and feed industries (Latham et al., 2023). The B-type
60 sesquiterpenoid deoxynivalenol (DON) is the most common FHB mycotoxin in European
61 food and feed wheat (Johns et al., 2022). The globally predominant DON producing species
62 is *Fusarium graminearum* (O'Donnell et al., 2000). During wheat spike colonisation, *F.*
63 *graminearum* undergoes a biphasic mode of infection. Initially, the fungus evades the host
64 immune response by growing between cells, causing no visible symptoms for ~3 days. This

65 is followed by an extended symptomatic stage marked by wheat tissue bleaching and
66 reduced grain development behind the advancing hyphal front (Brown et al., 2010, 2011).
67 STB disease on wheat leaves is caused by the fungus *Zymoseptoria tritici*. This fungus has
68 an extended symptomless stage of infection ~9 days, followed by a switch to symptomatic
69 disease (Goodwin et al., 2011; Steinberg, 2015). However, unlike *F. graminearum*, *Z. tritici*
70 colonisation is strictly confined to the sub-stomatal cavities and apoplastic spaces, without
71 ever invading host cells (Kema et al., 1996). Both pathogens are currently managed using
72 semi effective sources of host resistance mediated by major genes or QTLs (Brown et al.,
73 2015; Bai et al., 2018; Buerstmayr et al., 2020) as well as fungicide applications (Fones and
74 Gurr, 2015; Torriani et al., 2015; Buerstmayr et al., 2020; Kanja et al., 2021). But effective
75 control faces escalating issues caused by fungicide resistance (Estep et al., 2015; Lucas et
76 al., 2015; McDonald et al., 2019; de Chaves et al., 2022). There is a critical need to develop
77 new methods to combat these and other wheat fungal pathogens.

78 Understanding the genetic and molecular mechanisms driving host infection in numerous
79 interaction types continues to be a major goal of the international molecular plant pathology
80 community (Nelson, 2020; Jeger et al., 2021). Gene expression data can be organised into
81 co-expression networks, which group genes based on shared co-expression patterns.
82 Network representations are advantageous because these present biological data on a
83 systems-wide level, clustering genes in modules representative of specific stages or
84 functions. This modelling can be achieved using the weighted gene co-expression network
85 analysis (WGCNA) framework (Langfelder and Horvath, 2008). WGCNA has been
86 repeatedly applied to analyse fungal gene expression data. For instance, this approach has
87 been employed to identify effectors in *Magnaporthe oryzae* (Yan et al., 2023), shared genes
88 during *Fusarium oxysporum* infection across multiple hosts (Cai et al., 2022), and virulence
89 genes of *Colletotrichum siamense* (Liu et al., 2023). Although WGCNA has been used to
90 study wheat host responses to *F. graminearum* infection (Kugler et al., 2013; Pan et al.,
91 2018) and responses of *F. graminearum* under *in vitro* stress (L. Zhang et al., 2022; Park et

92 al., 2023), there has been no study of wheat-*F. graminearum* co-expression profiles during
93 infection.

94 To gain deeper insight on the expression patterns of genes during the different stages of the
95 *F. graminearum* infection the WGCNA framework was used to generate a fungal
96 pathogen/wheat dual co-expression network. Significantly, this framework can facilitate the
97 correlation of both fungal and host plant expression (Mateus et al., 2019). Within this
98 approach, genes are grouped into modules based on shared co-expression patterns
99 separately for the pathogen and the host. Modules are then correlated between the
100 pathogen and host networks to predict shared expression dynamics. In this study, correlated
101 expression between a mycotoxin gene-enriched fungal module and a detoxification gene-
102 enriched wheat module, validated the host-pathogen network. The study then focused on the
103 unique fungal module F16, characterised by high expression levels during the earliest
104 symptomless infection stage, and led to the discovery of *FgKnr4*. A subsequent
105 comprehensive experimental analysis revealed the pivotal role of *FgKnr4* in various
106 biological processes, including morphogenesis, growth, cell wall stress tolerance, and
107 virulence in *F. graminearum*. The *Knr4* gene is not restricted to *F. graminearum* but is
108 distributed widely across the fungal kingdom and is absent in other Eukaryotes. The various
109 mutant phenotypes observed in the *F. graminearum* $\Delta Fgknr4$ strain were replicated upon
110 deletion of the orthologous gene in the wheat pathogen *Z. tritici*. Overall, this study highlights
111 the value of using network analyses to model spatio-temporal pathogen-host interactions
112 and to identify novel conserved genes associated with virulence.

113

114 **Results**

115 **Generation of a dual *F. graminearum*-wheat co-expression** 116 **network**

117 *F. graminearum* floral infections can be divided into symptomatic or symptomless stages of
118 infection. Disease spread through the rachis internodes (RI) can be further broken down to
119 four different key stages of infection. Namely early symptomless (RI7-8), late symptomless
120 (RI5-6), early symptomatic (RI3-4), and late symptomatic (RI1-2) infection (**Figure 1A**). A
121 spatio-temporal transcriptomics dataset of *F. graminearum* floral infection of the susceptible
122 wheat cultivar Bobwhite, which distinguishes between these key distinct stages, was
123 previously generated (Dilks et al., 2019). This dataset also included spikelet tissue (SP)
124 sampled at 3 (early symptomatic) and 7 days post-infection (dpi) (late symptomatic). The
125 WGCNA framework (Zhang and Horvath, 2005; Langfelder and Horvath, 2008) was used to
126 construct a dual co-expression network to model fungal pathogen/crop interaction in wheat
127 using this dataset.

128 Normalised counts were used to generate two distinct networks: one for *F. graminearum* and
129 another for *T. aestivum*. The *F. graminearum* network consisted of 10,189 genes organised
130 into 18 modules (with 2629 – 60 genes per module), while the *T. aestivum* network consisted
131 of 47,458 genes distributed among 25 modules (with 23063 – 83 genes per module) (**Figure**
132 **2 – figure supplement 1, Supplementary File S1**). Both networks met scale free model
133 criteria at their selected soft thresholding power (**Figure 2 – figure supplement 2 A-B**). The
134 examination of module quality statistics found that each module within both networks were of
135 a high quality (Z-Summary > 10), with the exception of F16 (Z-Summary = 9.67), which still
136 markedly surpasses the minimum Z-Summary score of > 2 (Langfelder et al., 2011) (**Figure**
137 **2 – figure supplement 2C**). This indicates a substantial preservation of modules compared
138 to a random selection of all network genes. Additionally, preservation statistic calculations
139 confirmed that all modules maintain preservation (Z-summary > 2) across both networks with
140 all modules of the wheat network and the majority of the fungal modules (11/18) having
141 strong preservation (Z-summary > 10) (**Figure 2 – figure supplement 2D**). These findings
142 suggest a consistent preservation of within-network topology across modules (Langfelder et
143 al., 2011). For each module, a single summarised expression pattern, the eigengene value,

144 was calculated. The fungal and wheat modules were correlated by their eigengene
145 expression values, and modules displaying significant correlation ($p \geq 0.001$) formed the
146 dual co-expression network (**Figure 2A**).

147 To gain insight into the function of individual modules, a Gene Ontology (GO) enrichment
148 analysis was performed for both network sets (**Figure 2D-E, Figure 2 – figure supplement**
149 **1**). To confirm these enrichment patterns were not due to chance, a random network was
150 generated for both the fungal and wheat datasets. No significant enrichment was found for
151 the random wheat network and fungal network.

152 Among the eight wheat modules within the dual co-expression network, five of them were
153 significantly enriched for disease resistance genes (TO:0000112, $p \leq 0.05$) and one was
154 specifically enriched for wheat stripe rust resistance genes (TO:0020055) (**Figure 2E**),
155 suggesting the wheat modules in the network are needed for plant defence. One of these
156 wheat modules, W12, was significantly enriched in the GO terms detoxification
157 (GO:0098754; $p = 7.13 \times 10^{-7}$) and response to toxic substances (GO:0009636; $p = 2.11 \times$
158 10^{-6}). This module was correlated to the fungal module F12, which was enriched in genes
159 belonging to the trichothecene biosynthesis (*TRI*) gene cluster ($p = 1.92 \times 10^{-4}$) and for the
160 GO term terpenoid biosynthesis (GO:0016114 ; $p = 0.00085$) (**Figure 2D, Table 1**). Notably,
161 the module F12 was most highly expressed in the late symptomless stage of infection.
162 Expression of this module then rapidly decreases during the symptomatic stages of infection.
163 Module F12 therefore appears to be positioned specifically at the transition between the late
164 symptomless stage and the early symptomatic stage. The production of the DON mycotoxin
165 is essential for the transition to the extensive symptomatic stage (Cuzick et al., 2008; Jansen
166 et al., 2005). DON inhibits protein translation, which then eventually leads to cell death and
167 the bleached phenotype distinctive of symptomatic *F. graminearum* infection (Desmond et
168 al., 2008; Arunachalam and Doohan, 2013). High expression of module F12 in the
169 symptomless stage is also supported by previous data which found that genes involved in
170 mycotoxin biosynthesis are highly expressed in symptomless wheat tissue (Brown et al.,

171 2017). The correlation with the wheat module W12 therefore implies that detoxification
172 genes in the module are being expressed in response to production of fungal mycotoxins.
173 Interestingly, the fungal module F10 contains genes that are highly expressed in the earliest
174 and latest stages of *F. graminearum* infection, but not intermediate stages (**Figure 4**). The
175 fungal module F10 includes the Killer toxin 4 genes (*KP4L*) -1, -2, and -3. These genes also
176 have some of the highest module membership scores (>0.90) within the module. The *KP4L*
177 genes are necessary for virulence and expressed during both self and non-self interactions
178 (**Table 1**). It is suggested that *KP4L* proteins provide *F. graminearum* with a competitive
179 advantage when occupying new niches (Vicente et al., 2022), which would explain their
180 expression during the earliest stage of infection. High expression during late infection may
181 be necessary for intraspecific interactions, when the fungus is coordinating growth at a high
182 fungal density.

183 The stress-responsive mitogen-activated protein kinase *FgOS-2* is a key regulator in *F.*
184 *graminearum* and acts upstream of the ATF/CREB-activating transcription factor *FgAtf-1*
185 (**Table 1**). Both *FgOS-2* and *FgAtf-1* cluster in module F10. These proteins are involved in
186 broad functions, including secondary metabolite production, sexual reproduction, and stress
187 tolerance (Nguyen et al., 2013). Module F10 also contains two hydrophobin genes, *FgHyd3*
188 and *FgHyd5*. *FgHyd3* is necessary for attachment to hydrophobic surfaces, while both genes
189 are necessary for the production of aerial mycelia (**Table 1**). These genes are likely to play a
190 crucial role during early infection for surface attachment and are possibly expressed again
191 during the late stage of infection to facilitate the production of aerial mycelia.

192 The fungal module F10 is correlated with the wheat module W06 ($R = 0.85$, $p = 6 \times 10^{-6}$),
193 which is enriched in protein catabolism (GO:0010498; $p = 1.60 \times 10^{-19}$) and autophagy
194 (GO:0006914; $p = 2.31 \times 10^{-4}$) genes (**Table 1**). Autophagy plays a dual role in plant
195 immunity where it is involved in immune signalling and programmed cell death to restrict
196 pathogen spread, but also in response to pathogen induced necrotic cell death (Sertsuvalkul
197 et al., 2022). Therefore, it is likely these genes are expressed during early infection as an

198 immediate immune response and then expressed again in highly colonised tissue for late-
199 stage necrotrophic damage control.

200

201 **Wheat genes in module W12 are expressed in response to** 202 **DON production**

203 To validate the correlation between modules F12 and W12 (**Figure 3A**), expression of wheat
204 genes in the detoxification module W12 in response to *F. graminearum* infection without
205 DON was examined. This was achieved by inoculating wheat plants with either the wild-type
206 *F. graminearum* reference strain PH-1, or the DON deficient $\Delta Fgtri5$ mutant strain generated
207 in the PH-1 background. Expression of three wheat genes was studied, including two
208 phenylalanine ammonia-lyases (*PAL1* and 2; TraesCS4A02G401300 and
209 TraesCS2D02G377200) which were annotated with the term disease resistance
210 (TO:0000112), and a predicted transmembrane exporter, detoxification gene 16 (*DTX16*;
211 TraesCS5B02G371100).

212 The first two rachis internodes below the point of inoculation (POI) were sampled at 3 days
213 post inoculation (dpi). Levels of *FgActin* cDNA were not significantly different between
214 treatments (**Figure 3B**). Expression of the three wheat genes from module W12 was
215 significantly lower in the $\Delta Fgtri5$ infected samples relative to wild-type infection (**Figure 3C**).
216 This indicates that expression of genes in module W12 is correlated with DON production,
217 thereby supporting the correlated co-expression patterns observed between modules of the
218 two networks.

219 **Dual co-expression networks as a tool to identify key** 220 **genes necessary for virulence**

221 To pinpoint *F. graminearum* genes that are necessary for virulence, the stage specific
222 expression patterns of each module was examined (**Figure 4, Figure 4 – figure**
223 **supplement 1**). The module F16 is uniquely highly expressed during the earliest stages of
224 infection, with markedly decreased expression at all the other stages of infection. This
225 module is highly correlated to two wheat modules. These are W01 ($R = 0.91$; $p = 5 \times 10^{-7}$)
226 and W05 ($R = 0.85$, $p = 2 \times 10^{-5}$). W01 is the largest wheat module and is enriched for
227 defence response genes (GO:0006952; $p = 3.60 \times 10^{-08}$), but also maintenance genes which
228 include photosynthesis (GO:0015979; $p = 4.59 \times 10^{-29}$) and RNA modification (GO:0009451;
229 $p = 1.42 \times 10^{-47}$) GO terms. The wheat module W05 is enriched for disease resistance
230 (TO:0000112, $p = 2.55 \times 10^{-178}$), suggesting that despite the continued symptomless
231 infection the host is already expressing genes for defence. Four genes in module F16 result
232 in reduced virulence when individually deleted. These are *FgNPC1* (sterol trafficking)
233 (Breakspear et al., 2011), *FgSrp2* (mRNA splicing) (Zhang et al., 2020), and the transcription
234 factors *Gzcon7* and *Gzc2h045* (Son et al., 2011) (**Table 1, Supplementary File S2**).
235 However, no gene deletion mutants exhibiting a loss of pathogenicity have yet been
236 identified within this module, even though the eigengene expression pattern clearly indicates
237 an association with the early establishment of the fungus in this key host tissue.

238 To identify genes in F16 that are likely involved in virulence, the 74 genes within this module
239 were examined. Key genes were defined as those exhibiting elevated module membership
240 (MM) within the module, which were also strongly correlated ($R > |0.70|$) with corresponding
241 wheat modules. Genes with a high MM value have expression patterns closely aligned with
242 the module's overall eigengene expression and are the most representative of the module.

243 The initial candidate gene list was selected by starting with the 15 key genes with the highest
244 MM within the module. Genes were then excluded that were likely to have functional
245 redundancy (i.e. belonged to a gene family or had ancient paralogues within PH-1) to avoid
246 compensatory effects when performing single gene deletion (**Supplementary Table S1**).
247 Ultimately, only two genes met these criteria: FGRAMPH1_OT23707 and

248 FGRAMPH1_01T27545. FGRAMPH1_01T27545 has been previously characterised as the
249 Niemann–Pick type C gene (*FgNPC1*). *FgNPC1* is necessary for sterol trafficking, with its
250 deletion resulting in ergosterol accumulation within the vacuole and a reduced virulence
251 upon wheat infection (Breakspear et al., 2011). Orthologue analysis identified that the
252 FGRAMPH1_0T23707 gene was a 1:1 orthologue of Killer-nine resistant 4 (Knr4) in
253 *Saccharomyces cerevisiae* (Martin et al., 1999), therefore the orthologue in *F. graminearum*
254 is henceforth referred to as *FgKnr4*.

255 ***FgKnr4*, a key gene of module F16, is necessary for**

256 **establishment of fungal infection**

257 *FgKnr4* was deleted using a split hygromycin replacement cassette (**Figure 6 – figure**
258 **supplement 1 A-B**). *T. aestivum* cv. Bobwhite was inoculated at anthesis with three
259 independent $\Delta Fgknr4$ transformants. No symptomatic disease progression past the
260 inoculated spikelets was observed with each $\Delta Fgknr4$ transformant (**Figure 5 A-B**). While
261 the inoculated spikelets developed symptoms, these did not exhibit full bleaching of the
262 spikelet characteristic of FHB infection. Instead, eye-shaped lesions formed akin to those
263 evident following $\Delta Fgtri5$ mutant infection (**Figure 5C**) (Cuzick et al., 2008). Plating of
264 surface sterilised wheat dissected into its constituent parts revealed the absence of fungal
265 growth in un-inoculated spikelets (**Figure 5 – figure supplement 1**). Nevertheless, browning
266 was noted in the rachis tissue immediately adjacent to the point inoculated spikelet,
267 accompanied by fungal growth. However, this colonisation did not occur past the rachis
268 internode of the 3rd spikelet. These data suggest that, despite entering the rachis, the
269 $\Delta Fgknr4$ mutant is unable to grow through the rachis node tissue and re-enter other
270 spikelets. Microscopic examination revealed a more pronounced plant defence response to
271 $\Delta Fgknr4$ infection. This was characterised by a visibly reduced fungal burden (**Figure 5D**).
272 Despite highly reduced virulence, DON mycotoxin was detected in the inoculated spikelet
273 and attached rachis internodes (≥ 0.2 ppm). However, DON was undetectable in the

274 neighbouring uninoculated spikelet (< 0.2 ppm). Complementation of the mutant with wild-
275 type *FgKnr4* restored virulence to wild-type levels (**Figure 5 E-F**).

276

277 ***FgKnr4* influences cell wall structure, stress resistance,** 278 **and growth**

279 *In vitro* growth of $\Delta Fgknr4$ was examined by culturing the fungus on both high or low nutrient
280 agar. In both conditions a decreased growth rate relative to the wild-type was apparent
281 (**Figure 6A, Figure 6 – figure supplement 1 and 2**). In addition to this, conidia of $\Delta Fgknr4$
282 appear smaller than wild-type (**Figure 6 – figure supplement 3 A, C**). Despite these
283 morphological differences $\Delta Fgknr4$ retains the ability to produce perithecia and ascospores,
284 albeit 8 days later than the wild-type (**Figure 6 – figure supplement 3 D-G**).

285 Stresses encountered by the fungus during *in planta* infection were mimicked *in vitro* using
286 chemical stressors. $\Delta Fgknr4$ had increased susceptibility to osmotic stress (1.5M NaCl),
287 oxidative stress (H₂O₂), and calcofluor white induced cell wall damage compared to the wild-
288 type and complemented strains (**Figure 6A, Figure 6 – figure supplement 1C & 2C**).

289 These susceptibilities may be due to changes in the cell wall structure of the $\Delta Fgknr4$ strain.
290 Corroborating this hypothesis, staining for chitin found an irregular deposition of chitin on the
291 $\Delta Fgknr4$ conidial cell wall, specifically along the tips and septa of the conidia (**Figure 6B,**
292 **Figure 6 – figure supplement 4**). Furthermore, an irregular cell wall structure was observed
293 upon transmission electron microscopy (TEM) analysis of the $\Delta Fgknr4$ conidia, indicative of
294 an abnormal cell wall composition (**Figure 6C, Figure 6 – figure supplement 5**).

295 The *FgKnr4* (F16) module was correlated with the wheat module W05, which exhibits a
296 significant enrichment in the term oxidative stress (TO: 0002657; $p = 3.88 \times 10^{-34}$) that
297 encompasses a total of 1143 genes. Among these genes are two respiratory burst oxidase
298 homologues (RBOH), specifically a predicted homolog of RBOF (TraesCS1A02G347700)

299 and RBOHE (TraesCS5D02G222100), along with predicted catalase homologues, CAT3
300 (TraesCS7B02G473400) (Ghorbel et al., 2023; Yan Zhang et al., 2022), and two CAT4
301 genes (TraesCS5B02G023300, TraesCS5D03G0079400) (Andleeb et al., 2022). W05 is
302 also enriched for sodium content (TO: 0000608; $p = 0.00014$) and salt tolerance (TO:
303 0006001; $p = 3.00 \times 10^{-18}$). The necessity of a functional *FgKnr4* gene in oxidative and
304 osmotic stress tolerance (**Figure 6A, Figure 6 – figure supplement 1C & 2C**) suggests that
305 *FgKnr4* is critical during this early infection stage, where the fungus confronts hydrogen
306 peroxide and osmotic stress induced by the plant.

307 The involvement of *FgKnr4* in cell wall metabolism was further studied by examining its
308 effect on the cell wall integrity pathway (CWI). The fungal CWI pathway is triggered in
309 response to various stresses (e.g. oxidative stress, osmotic pressure, cell wall damage)
310 (Dichtl et al., 2016) and in *F. graminearum* is activated through the phosphorylation of the
311 MAP-kinase (MAPK) *FgMGV1* (Hou et al., 2002; Yun et al., 2014). A Western blot was run
312 on mycelium samples grown with and without a cell wall stress (calcofluor white).
313 Constitutive activation of MGV1 in the absence of stress and increased phosphorylation
314 under stress was observed in $\Delta Fgknr4$ when compared to the wild-type (**Figure 6D-E**). This
315 finding is consistent with previous observations in *S. cerevisiae* (Martin-Yken et al., 2003).
316 This reinforces the biological function of *FgKnr4*, suggesting an involvement in fungal stress
317 responses and cell wall morphology in *F. graminearum*.

318 **The orthologous gene in the wheat pathogen *Zymoseptoria*** 319 ***tritici* is also important for cell wall integrity and virulence** 320 **on wheat**

321 Analysis of the Knr4 protein conservation found that orthologues were highly distributed
322 across the Dikarya, occurring in both Ascomycota and Basidiomycota (**Figure 7**). Notably,
323 no orthologues of the gene were found in other Eukaryotes, highlighting its specificity to the

324 fungal lifestyle. This high level of conservation across fungi suggests that phenotypes
325 observed in *F. graminearum* may also be conserved in other economically significant
326 pathogenic fungi.

327 The orthologous *Knr4* gene in another wheat fungal pathogen *Z. tritici* (*ZtKnr4*,
328 Mycgr3G105330) was disrupted to test for conserved gene function. Despite the
329 phylogenetic distance between the two fungi, the FgKnr4 and ZtKnr4 proteins share 43.5%
330 pairwise identity. Mirroring the phenotype observed in *F. graminearum*, reduced virulence
331 (chlorosis but limited to no necrosis) was observed when wheat leaves were inoculated with
332 $\Delta Ztknr4$ (**Figure 8A**). In addition to this the $\Delta Ztknr4$ mutant was susceptible to calcofluor
333 white induced cell wall stress and exhibited reduced hyphal branching (**Figure 8B-C**). These
334 results highlight the potential of employing the *Fusarium*-wheat dual co-expression approach
335 to gain insights into fungal-plant interactions, both within *Fusarium* species and across the
336 fungal kingdom.

337

338 Discussion

339 The generated dual *F. graminearum*-wheat co-expression network was successfully used to
340 identify a gene necessary for virulence. By analysing stage-specific modules of infection,
341 module F16 was identified, which exhibited high gene expression levels during the
342 symptomless stage of FHB infection. Within this module, the gene *FgKnr4* was found to
343 have a high module membership score, indicating its central role in the module.

344 Experimental validation showed that *FgKnr4* is essential for responding to chemical
345 compounds that induce cell wall stress, for early establishment of *in planta* infection, and
346 subsequent disease progression in wheat spikes. Similarly, the deletion of *Knr4* in another
347 pathogenic species, namely *Z. tritici* resulted in a reduced virulence phenotype in leaves and
348 displayed a comparable cell wall stress phenotype. This highlights the utility of pathogen-

349 host co-expression network analysis in identifying conserved virulence genes across wheat
350 fungal pathogens.

351 The predictions from the WGCNA were validated for the F12-W12 correlation through the
352 experimental confirmation of the co-regulation of the *Fusarium* trichothecene mycotoxin and
353 wheat detoxification genes during infection. For *Fusarium*, module F12 was of exceptionally
354 high interest because of its positioning specifically at the transition between the late
355 symptomless stage and the early symptomatic stage. For wheat genes in the correlated
356 module W12, the studied genes included two phenylalanine ammonia-lyases (*PAL1* and *2*)
357 along with a predicted detoxifying efflux transporter (*TaDTX16*). Although *TaPAL1* and *2*
358 have not been previously studied for their direct involvement in disease resistance in the
359 wheat - *Fusarium* interaction, the *PAL* gene family is known to be associated with disease
360 resistance and other phenotypes (Duba et al., 2019). In multiple plant species (including
361 *Arabidopsis*, pepper (*Capsicum annuum*), and rice (*Oryzae sativa*)), *PAL* is induced in
362 response to biotic and abiotic stresses, which includes pathogen induced stress (Hahlbrock
363 and Scheel, 1989; Kim and Hwang, 2014; Tonnessen et al., 2015; Chen et al., 2017), and in
364 numerous genetically incompatible host-pathogen interactions mediated by cognate R-Avr
365 proteins including responses to fungi (Maher et al., 1994; Ramarosan et al., 2022). *TaDTX16*
366 is part of the multidrug and toxic compound extrusion (MATE) gene family and was named
367 after its orthologue in *Arabidopsis thaliana* (Li et al., 2002). DTX/MATE genes take part in
368 heavy metal and lethal compound detoxification in plants and could be involved in mycotoxin
369 detoxification (Perincherry et al., 2019). Previously, a wheat DTX gene was reported to be
370 highly expressed in resistant cultivars of wheat compared to a susceptible wheat cultivar
371 when infected with *F. graminearum* (Pan et al., 2018). Furthermore, *TaDTX16* is located on
372 chromosome 5BL within an interval harbouring a resistance QTL for defence against the
373 necrotrophic fungal disease *Septoria nodorum* blotch (Li et al., 2021).

374 The characterisation of *FgKnr4*, underscores the importance of identifying genes necessary
375 for full virulence through gene expression studies. This approach is essential because

376 predicting the pathogenic potential of *Fusarium* species based solely on comparative
377 genomics is challenging due to the absence of significant differences in secreted effector
378 proteins, carbohydrate-active enzymes, or gene repertoires between pathogenic and
379 endophytic strains of *Fusarium* and Fusarioid species (Hill et al., 2022). *FgKnr4* was
380 investigated further for its multifaceted roles in growth, stress response, and cell wall
381 integrity. Supporting previous findings in *Fusarium asiaticum* (Yu Zhang et al., 2022), this
382 study demonstrates that *FgKnr4* is involved in regulating growth rate, conidial spore
383 morphology, and sensitivity to osmotic and oxidative stresses, as well as virulence and cell
384 wall stress tolerance in *F. graminearum*. Moreover, this study establishes that *Knr4*
385 influences the well-studied cytoplasmically located *Mgv1* cell wall integrity (CWI) MAPK
386 pathway (Xu et al., 2022), resulting in visible abnormalities of the conidial cell wall (**Figure**
387 **6C, Figure 6 – figure supplement 5**). The cell wall integrity pathway in *F. graminearum* is
388 well-characterised, with each MAP-kinase in the cascade having been identified, studied,
389 and shown to have roles in virulence and/or asexual and sexual spore formation (Hou et al.,
390 2002; Jenczmionka et al., 2003; Urban et al., 2003; Zheng et al., 2012). Through
391 experimental validation, our findings reveal an additional layer of control within the *F.*
392 *graminearum* cell wall integrity pathway mediated by *FgKnr4*. This discovery contributes to
393 and further improves our understanding of the regulatory mechanisms governing cell wall
394 integrity in *F. graminearum*. This new finding also, offers the first insights into the regulatory
395 effects of *Knr4* in a filamentous fungus. This additional knowledge aids the development of
396 novel strategies to mitigate losses caused by FHB disease and DON contamination.

397 *Z. tritici* possesses one of the most expansive publicly available eukaryotic pangenomes,
398 with approximately 42% of its genes categorised as accessory (Plissonneau et al., 2018).
399 *ZtKnr4* is part of the core *Z. tritici* genome of the European pangenome (Chen et al., 2023)
400 and designated within the core orthogroup OG0008320 within the global (Europe, Asia,
401 North and South America, Australia, and Africa) pangenome (Badet et al., 2020). Given the
402 highly variable nature of accessory chromosomes in *Z. tritici*, the assignment of *ZtKnr4* to the

403 core genome in two separate pangenomic analyses underscores its importance in fungal
404 physiology. *ZtKnr4* is also expressed throughout the wheat infection process (Rudd et al.,
405 2015). Disruption of the gene resulting in a reduced virulence phenotype reinforces the
406 potential of *ZtKnr4* as a candidate target for fungicide development, emphasising its
407 significance in combating *Z. tritici* infections and mitigating agricultural losses. Despite the
408 ever present global importance of STB disease for many decades (Dean et al., 2012; Savary
409 et al., 2019) *Z. tritici* has far fewer functionally characterised genes, with only 99 genes with
410 a characterised phenotype within the Pathogen Host-Interactions database and only 50 of
411 these genes associated with a loss in pathogenicity or reduced virulence (Urban et al., 2022;
412 Cuzick et al., 2023, <http://www.phi-base.org/>). The reduced virulence phenotype observed in
413 the *ZtKnr4* mutant therefore marks a valuable contribution to the characterisation of one of
414 the >9000 core genes across the known *Z. tritici* pangenomes (Badet et al., 2020; Chen et
415 al., 2023).

416 The high conservation and exclusivity of *Knr4* within the fungal kingdom, combined with its
417 absence in other eukaryotes and its conserved function across related species, suggest that
418 *Knr4* could be an ideal target for intervention. This could be achieved through the
419 development of chemical fungicides that disrupt the protein's function (Aamir et al., 2018) or
420 through the application of RNA interference techniques (Cools and Hammond-Kosack, 2013;
421 Machado et al., 2018; Mann et al., 2023). Stricter EU regulation of chemicals suitable for
422 fungicide use in agricultural, medical and/or veterinary settings (European Commission,
423 2022), combined with significant losses in fungicide efficacy due to the evolution of pathogen
424 populations means there is a pressing need to identify new target sites for control.
425 Therefore, this research not only advances our understanding of fungal virulence
426 mechanisms but also offers promising directions for the development of effective strategies
427 for disease control in agriculture.

428 **Materials and Methods**

429 Gene co-expression network analysis

430 RNA-seq reads from Dilks et al. (2019) were provided by Dr Neil Brown (European
431 Nucleotide Archive: PRJEB75530). Read quality was assessed with FastQC v. 0.11.9
432 (Andrews, 2010, <https://www.bioinformatics.babraham.ac.uk/projects/fastqc/>). Reads were
433 mapped to a combined Fusarium – wheat genome, consisting of v. 5 of the *Fusarium*
434 *graminearum* PH-1 genome (King et al., 2017a) and the high confidence (HC) transcripts of
435 the v. 2.1 of the International Wheat Genome Sequencing Consortium (IWGSC) *Triticum*
436 *aestivum* genome (Zhu et al., 2021). Genome indexing and read alignment were performed
437 using STAR aligner 2.7.8a. Soft clipping was turned off to prevent reads incorrectly mapping
438 to similar regions of the highly duplicated hexaploid wheat genome. Reads were filtered
439 using the filterByExpr function part of the R package Edge R v.3.32.1 (Robinson et al.,
440 2010). Counts were normalised separately for fungal and wheat reads by performing a
441 variance stabilising transformation (VST) using the DESeq2 v 1.30.1 R package (Love et al.,
442 2014) in R (v4.0. 2, <https://www.r-project.org/>).

443 The VST normalised counts were filtered to remove any excessive missing values using the
444 function goodSamplesGenesMS in the WGCNA R package (Langfelder and Horvath, 2008).
445 Standard methods were implemented to generate the network using the WGCNA R
446 package, with the following parameters. A signed-hybrid network was constructed using the
447 filtered counts. The soft thresholding power (β) was uniquely selected per network according
448 to scale free model criteria (Zhang and Horvath, 2005), where $\beta = 9$ for the fungal network
449 and $\beta = 18$ for the wheat network (**Figure 2 – figure supplement 2**). A deepSplit of 3 was
450 paired with a standard cutheight of 0.25. A minimum module size of 50 was selected to
451 minimise potential transcriptional noise when assigning modules using smaller datasets
452 (Oldham, 2014; Walsh et al., 2016). The function multiSetMEs from the WGCNA package
453 was used to calculate module eigengene expression. Module eigengenes with similar
454 expression profiles were then merged.

455 Module quality and preservation was calculated using the function `modulePreservation`
456 present in the WGCNA R package (Langfelder and Horvath, 2008; Langfelder et al., 2011).
457 When calculating module preservation, the original wheat or fungal network was considered
458 the reference network. Then 50 different test networks were created, each built upon
459 randomly resampling (with replacement) a proportion of samples from the original dataset.
460 The average preservation metrics (i.e. Z-score) between the original network and the 50 test
461 networks was calculated for both the fungal and wheat networks.

462 **Module Enrichment an Annotation**

463 Gene ontology (GO) annotations of the v. 5 PH-1 genome (GCA_900044135.1) were
464 generated using Blast2GO v .5 (Götz et al., 2008). Enrichment was calculated using a
465 background set of all genes present in the fungal network. GO annotations for the IWGSC
466 v.2.1 genome were provided by Dr Keywan Hassani-Pak of the KnetMiner team (Hassani-
467 Pak et al., 2021). This was generated by performing a BLASTx search on the NCBI nb
468 database using DIAMOND v 2.0.13-GCC-11.2.0 (Buchfink et al., 2015), then Blast2GO v.5
469 was used to annotate the BLAST hits with GO terms. GO term enrichment was calculated for
470 each high level GO ontology (Biological Process, Molecular Function and Cellular
471 Component) using the R package topGO v 2.46.0 (Alexa and Rahnenfuhrer, 2009).

472 Plant Trait Ontology (TO) (Cooper et al., 2024) enrichment analysis was performed using
473 annotations derived from the KnetMiner knowledge graph (release 51) for wheat (Hassani-
474 Pak et al., 2021) and KnetMiner datasets and enrichment analysis notebooks are available
475 at <https://github.com/Rothamsted/knetgraphs-gene-traits/>. Predicted effectors were
476 determined using EffectorP v.3.0 (Sperschneider and Dodds, 2022). Alongside this,
477 predictions to identify extracellularly localised genes were done using SignalP v6.0 (Teufel et
478 al., 2022). Custom *F. graminearum* gene set enrichment of the network modules was
479 calculated by performing a Fisher's exact test using all the genes in the fungal network as
480 the background gene set. A BH correction was calculated for both GO and custom

481 enrichments (Benjamini and Hochberg, 1995). Modules were deemed significantly enriched
482 if $P\text{-corr} < 0.05$.

483 Gene lists included in the GSEA consisted of predicted secreted effector proteins, alongside
484 known gene families associated with virulence, such as biological metabolite clusters
485 (BMCs) (Sieber et al., 2014), polyketide synthases (Gaffoor et al., 2005), protein kinases
486 (Wang et al., 2011) and transcription factors (Son et al., 2011). Due to their well-established
487 importance in *F. graminearum* pathology, a separate enrichment for genes of the *TRI* gene
488 cluster was also performed.

489 Annotation from PHI-base was obtained by mapping genes to version PHI-base (v4.16)
490 annotation using UniProt gene IDs and any through Decypher Tera-Blast™ P (TimeLogic,
491 Inc. Carlsbad, California, USA) (E-value = 0) against the PHI-base (v4.16) BLAST database
492 (Urban et al., 2022; Cuzick et al., 2023).

493 **Fungal material and growth conditions**

494 *F. graminearum* strains were cultured and conidia prepared as previously described (Brown
495 et al., 2010). Fungal strains were grown for 4 days on nutrient-rich potato dextrose agar
496 (PDA), nutrient-poor synthetic nutrient agar (SNA; 0.1% KH₂PO₄, 0.1% KNO₃, 0.1%
497 MgSO₄·7H₂O, 0.05% KCL, 0.02% glucose, 0.02% sucrose and 2% agar) and PDA with
498 different cell wall stresses. This included 150 µg/ml calcofluor white, 1.5mM H₂O₂, and 1.5M
499 NaCl. Plates were point inoculated with 20 µl of 4-fold dilution series starting with 1 x 10⁶
500 conidia/ml. For the growth rate assay, fungi were grown on PDA and measurements were
501 taken after 3, 5, and 7 days. Surface sterilisation of wheat spikes was performed by
502 submerging single wheat spikelets in 1/8 diluted thin bleach for 3 min, followed by three
503 washes with distilled H₂O. Dissection was done using a razor blade to separate the point
504 inoculated spikelets and adjacent spikelets (**Figure 5 – supplement 1**). Wheat tissue was
505 placed on SNA and images were taken after a 3-day incubation at room temperature in the
506 dark. Perithecia induction was achieved as described in Cavinder et al. (2019). All plate

507 images were taken using an Olympus OM-D camera with a 60mm ED M.Zuiko macro lens.
508 Conidia and ascospore images were taken using the Axiomager 2 (Zeiss, Oberkochen,
509 Germany) under brightfield illumination. Conidia lengths (N = 50) and perithecia heights (N =
510 40) were measured using ImageJ (Schneider et al., 2012).

511 ***Fusarium graminearum* genetic manipulations**

512 The *FgKnr4* gene was deleted through split marker-mediated transformation targeted fungal
513 replacement with the hygromycin resistance cassette by homologous recombination (Yu et
514 al., 2004). *F. graminearum* gene deletion construct assembly and fungal transformation was
515 performed following methods outlined in King et al., 2017b. Primers were designed for the
516 fusion of the 5' and 3' constructs using the NEBuilder® Assembly Tool v.1
517 (<https://nebulderv1.neb.com/>). Using the Gibson Master Mix (New England Biolabs, UK) the
518 paired split marker fragments were ligated into the pGEM® - T Easy Vector (Promega, UK)
519 then transformed into DH5α competent *Escherichia coli* (C2987H, New England Biolabs,
520 UK) following standard manufacturer protocol. Diagnostic PCRs were done using DreamTaq
521 polymerase (ThermoFisher, UK) and standard cycling conditions. For the single gene
522 deletion, in three separate transformants two diagnostic PCRs detect the presence of the
523 replacement cassette flanks (P3-4, P5-6) and the absence of the wild-type gene (P1-2)
524 **(Figure 6 – figure supplement 1 A-B)**. Complementation was performed following the
525 protocol developed by Darino et al. (2024). Diagnostic PCRs for the complemented strains
526 involved amplification of insertion cassette flanks (P7-8; P1-9), absence of short 868 bp
527 empty intragenic locus amplicon (P11-P12), and test for heterozygosity of geneticin gene
528 (P13-P14) **(Figure 6 – figure supplement 2 A-B)**. A full primer list is available in
529 Supplementary File S3.

530 **Wheat host inoculation**

531 The susceptible spring wheat (*T. aestivum*) cultivar, Bobwhite, was grown to anthesis. The
532 5th and 6th spikelets from the top of the wheat spike were inoculated on both sides using 5
533 μl of 5×10^5 conidia/ml. Each treatment included 10 separate wheat plants ($N = 10$). After
534 inoculation, plants were kept in a high humidity chamber for 48 h in the dark. Disease
535 progression was documented every two days by scoring the number of bleached spikelets.
536 At 15 dpi wheat spikelet tissue and the adjacent rachis internode was separated, frozen in
537 liquid nitrogen, and ground to form a fine powder. The presence of DON mycotoxin was
538 assessed using the Deoxynivalenol (DON) Plate Kit (Cat. 20-0016, Beacon Analytical
539 Systems Inc., USA) following standard protocol. This experiment was replicated with three
540 biological replicates per treatment ($N = 3$). All *F. graminearum* infected plant images were
541 taken using an Olympus OM-D camera using a 60mm ED M.Zuiko macro lens.

542

543 For resin dissection microscopy wheat cv. Bobwhite was inoculated 7th and 8th true spikelets
544 from base inoculated each side w/ 5×10^5 spores /ml in dH₂O. After inoculation, plants were
545 kept in a high humidity chamber for 48 h in the dark. Lemma tissues were excised from
546 infected spikelets at 7 dpi, fixed in a 4% paraformaldehyde, 2.5% glutaraldehyde solution
547 with 0.05M Sorensen's phosphate buffer ($\text{NaH}_2\text{PO}_4:\text{Na}_2\text{HPO}_4$, pH 7.0). Samples then
548 underwent 3 further buffer washes, a subsequent ethanol dehydration protocol (0-100%
549 EtOH) over 48hrs and LR White resin (TAAB) infiltration diluted with dry ethanol at
550 increasing ratios (1:4, 2:3, 3:2, 4:1, 100%). Samples were inserted into capsules (TAAB) and
551 resin polymerised at 60°C for 16 hours in a nitrogen oven (TAAB). Ultra-thin 1 μm sections of
552 samples were cut on an ultramicrotome (Reichert-Jung, Ultracut) with glass knives, placed
553 onto glass polysine slides (Sigma Aldrich, UK), dried at 70°C, stained with 0.1% (w/v)
554 Toluidine Blue O and mounted in DPX mounting medium (Fisher Scientific). Stained sections
555 were imaged on a Zeiss Axioimager (AxioCam 512 color, Zeiss, Jena, Germany) light
556 microscope with brightfield illumination.

557 **Gene expression of module W12 genes**

558 Bobwhite wheat plants were point inoculated at anthesis with either wild-type PH-1, *ΔFgtri5*
559 or water only (Mock) following the protocol outlined in Dilks et al., (2019). Each experimental
560 condition was replicated in triplicate, with each replicate deriving from three pooled
561 independent wheat spikes. Tissues from rachis internodes 1 and 2 were sampled and frozen
562 in liquid nitrogen at 3 dpi. Frozen samples were ground and RNA was extracted using the
563 Monarch® Total RNA Miniprep Kit (NEB, UK). Equal amounts of RNA were used to
564 synthesise cDNA with Revertaid cDNA synthesis kit (ThermoScientific, UK). PowerTrack™
565 SYBR Green Master Mix (ThermoScientific, UK) was used for qPCR. Each biological
566 replicate included three technical replicates. All primers are provided in Supplementary File
567 S3.

568 **Western blot**

569 A 200 µl aliquot of a *F. graminearum* spore solution (1×10^6 spores/ml) was added to 10 ml
570 potato dextrose broth (PDB) at 27 °C. Calcofluor white was added to a concentration of 200
571 µg/ml after 24 h of incubation at 180 rpm. Twenty-four hours after the addition of the stress,
572 mycelium was harvested, flash frozen and freeze dried. To lyse the samples Y-PER Yeast
573 Protein Extraction Reagent (ThermoScientific, UK) was added to the freeze-dried samples at
574 1.5 ml per 150 mg tissue, alongside Protease Inhibitor Cocktail (100x) (ThermoScientific,
575 UK). Samples were lysed using the FastPrep-24™ machine for 20s (MP Biomedical, USA).
576 The supernatant was mixed with 5xSDS loading buffer (National Diagnostics, USA).
577 Equal amounts of protein (60 µg) were resolved on 8% SDS-PAGE gels (Mini-PROTEAN,
578 Bio-Rad, UK) and transferred on to a nitrocellulose membrane. Immunoblots were performed
579 by standard procedures using the Phospho-p44/42 MAPK (Erk1/2) (cat. #4370) and p44/42
580 MAPK (Erk1/2) (cat. #9102S) (Cell Signalling Technologies, USA) antibodies at their
581 specified dilutions. The blots were developed using ECL Plus Western Blotting Detection Kit

582 and images were acquired using Odyssey Imaging System (LI-COR Biosciences Ltd,
583 Cambridge, UK).

584 **Microscopic examination of cell wall**

585 Spores were induced by plating 200 µl of frozen spores (1×10^6) PDA and incubating plates
586 in for 3 days. For conventional transmission electron microscopy (TEM), fresh spores were
587 harvested the same day from the PDA plates and pellets were fixed in a mixture of 2.5%
588 glutaraldehyde and 4% Paraformaldehyde in Sorenson's buffer (SB) at pH 7.2 overnight at
589 4°C. The samples were rinsed in SB and post fixed in 1% osmium tetroxide for 60 min at
590 room temperature. The samples were dehydrated for 10 min per step into increasing
591 concentrations of alcohol (30%, 50%, 70%, 90% and final 100% $\times 3$). Subsequently, the pure
592 alcohol was replaced with propylene oxide, and the specimens were infiltrated with
593 increasing concentrations (25%, 50%, 75%, and 100%) of Spurr resin mixed with propylene
594 oxide for a minimum of 2 hr per step. The samples were embedded in pure, fresh Spurr resin
595 and polymerised at 60 °C for 24 hr. Ultrathin sections (70 nm) were cut using an
596 ultramicrotome (Leica UC7, Germany) and post-stained, first with uranyl acetate for 1 min and
597 then with Reynolds lead citrate for 2 min at room temperature, prior to observation using a
598 Transmission Electron Microscope (Jeol 2100plus, UK) operated at 200 kV.

599 *F. graminearum* spore solution (1×10^6 spores/ml) was stained with Wheat Germ Agglutinin,
600 Alexa Fluor™ 488 Conjugate (WGA) (10 µg/ml) for 10 minutes each. Samples were washed
601 three times in sterile distilled water after staining. A ZEISS 780 Confocal Laser Scanning
602 Microscope (ZEISS, Germany) was used to image spores.

603 **Phylogenetic tree construction**

604 Eggnogmapper-v5 (Huerta-Cepas et al., 2019) was used to map *FgKnr4* to the eggnog
605 Orthologue Group (OG) ENOG502QTAZ and generate the phylogenetic tree. The tree was

606 visualised and annotated using the interactive Tree of Life (iTOL) software (Letunic and
607 Bork, 2024).

608 **Functional characterisation of the *Knr4* orthologue in *Z.***

609 ***tritici***

610 Separate analyses using Orthologous Matrix (OMA) (Altenhoff et al., 2021) and
611 EggNOGmapper (Huerta-Cepas et al., 2019) identified a single orthologous sequence in the
612 genome of the *Z. tritici* isolate IPO323

613 (https://fungi.ensembl.org/Zymoseptoria_tritici/Info/Index) (Goodwin et al., 2011). The gene
614 has a Rothamsted gene model Id of ZtritIPO323_04g12347 (King et al., 2017b; Chen et al.,
615 2023) and is present on Chromosome 8 at start position 230142 bp. This maps to
616 Mycgr3P105330 in the current genome call on Joint Genome Institute (JGI) MycoCosm
617 (Goodwin et al., 2011).

618 Agrobacterium-mediated fungal transformation (Motteram et al., 2011) was performed to
619 generate a series of independent gene disruption mutants of *ZtKnr4*. Flanking sequences
620 and the hygromycin resistance gene were amplified from either genomic DNA or from
621 plasmid pCHYG and using Phusion polymerase (NEB, UK). Fragments were gel purified
622 using QIAquick Gel Extraction Kit (QIAGEN, UK) and assembled into the backbone (Kpn1
623 and BamH1 digested) of pCHYG by Gibson Assembly (NEB, UK). The resulting plasmids
624 were transformed into Agrobacterium strain AgL1 and fungal transformation of isolate
625 IPO323 was performed as per standard protocols (Motteram et al., 2011). Positive
626 transformants containing a disrupted *ZtKnr4* gene were identified by diagnostic PCR (**Figure**
627 **8 – figure supplement 1**). Complementation of the validated *ZtKnr4* mutant was performed
628 through Agrobacterium-mediated transformation with plasmid pCGEN (digested EcoR1 and
629 Kpn1) containing the native gene plus 1 kb upstream (5') and 300 bp (3') downstream
630 genomic DNA, amplified by Phusion PCR (NEB, UK).

631 Attached leaf virulence assays were performed as per standard protocols (Keon et al., 2007)
632 on wheat cultivar Riband. Leaf blades (N = 3) were inoculated with spore suspensions of $1 \times$
633 10^6 spores / ml in sterile water + 0.05% v:v Tween 20. Final disease assessments were
634 made 20 days after inoculation. *In vitro* hyphal growth assays were performed following
635 droplet inoculation of spore suspensions onto 1% Tap Water Agar (TWA) plates. Hyphal
636 growth morphologies were determined by light microscopy and / or photography 10 days
637 after inoculation. Calcofluor white sensitivity assays were performed to ascertain changes in
638 cell wall strength. For this, spore suspensions were inoculated onto YPD agar (Formedium,
639 UK) plates (control) and onto YPD agar plates containing 200 μ g / ml calcofluor white. Plates
640 were incubated at RT for 8 days and then growth was monitored and recorded by
641 photography. Images of *ZtKnr4* *in planta* and *in vitro* experiments were taken with a Nikon
642 D3200 camera.

643 **Data availability**

644 Full lists of all genes clustered into modules is available on
645 https://github.com/erikakroll/Fusarium-wheat_WGCNA. This includes comma
646 separated value (CSV) files for all genes in each module for both fungal and wheat
647 modules, which are annotated with Module Membership (MM) values, mean FPKM
648 values, InterPro annotation, Gene Ontology annotation, and Trait Ontology
649 annotation. Text documents containing module eigengene values and gene module
650 assignments are also available on the repository.

651

652 **References**

653 Aamir M, Singh VK, Dubey MK, Meena M, Kashyap SP, Katari SK, Upadhyay RS,
654 Umamaheswari A, Singh S. 2018. In silico Prediction, Characterization,

655 Molecular Docking, and Dynamic Studies on Fungal SDRs as Novel Targets
656 for Searching Potential Fungicides Against Fusarium Wilt in Tomato. *Front*
657 *Pharmacol* **9**:1038. doi:10.3389/fphar.2018.01038

658 AHDB. 2023. Risk assessment for fusarium mycotoxins in wheat | AHDB.
659 <https://ahdb.org.uk/mycotoxins>

660 Alexa A, Rahnenfuhrer J. 2009. Gene set enrichment analysis with topGO.
661 *Bioconductor Improv* **27**:1–26.

662 Altenhoff AM, Train C-M, Gilbert KJ, Mediratta I, Mendes de Farias T, Moi D, Nevers
663 Y, Radoykova H-S, Rossier V, Warwick Vesztröcy A, Glover NM, Dessimoz
664 C. 2021. OMA orthology in 2021: website overhaul, conserved isoforms,
665 ancestral gene order and more. *Nucleic Acids Res* **49**:D373–D379.
666 doi:10.1093/nar/gkaa1007

667 Andleeb T, Knight E, Borrill P. 2022. Wheat NAM genes regulate the majority of early
668 monocarpic senescence transcriptional changes including nitrogen
669 remobilization genes. *G3 GenesGenomesGenetics* **13**.
670 doi:10.1093/g3journal/jkac275

671 Andrews S. 2010. FastQC: a quality control tool for high throughput sequence data.

672 Armer V, Kroll E, Darino M, Urban M, Smith D, Hammond-Kosack K. 2024.
673 Navigating the Fusarium species complex: Host-Range Plasticity and
674 Genome Variations. Re-submitted post peer review for special issue in Fungal
675 Biology.

676 Arunachalam C, Doohan FM. 2013. Trichothecene toxicity in eukaryotes: Cellular
677 and molecular mechanisms in plants and animals. *Toxicol Lett* **217**:149–158.
678 doi:10.1016/j.toxlet.2012.12.003

679 Badet T, Oggenfuss U, Abraham L, McDonald BA, Croll D. 2020. A 19-isolate
680 reference-quality global pangenome for the fungal wheat pathogen
681 *Zymoseptoria tritici*. *BMC Biol* **18**:12. doi:10.1186/s12915-020-0744-3

682 Bai G, Su Z, Cai J. 2018. Wheat resistance to Fusarium head blight. *Can J Plant*
683 *Pathol*.

684 Benjamini Y, Hochberg Y. 1995. Controlling the False Discovery Rate: A Practical
685 and Powerful Approach to Multiple Testing. *J R Stat Soc Ser B Methodol*
686 **57**:289–300. doi:10.1111/j.2517-6161.1995.tb02031.x

687 Breakspear A, Pasquali M, Broz K, Dong Y, Kistler HC. 2011. Npc1 is involved in
688 sterol trafficking in the filamentous fungus *Fusarium graminearum*. *Fungal*
689 *Genet Biol FG B* **48**:725–730. doi:10.1016/j.fgb.2011.03.001

690 Brown JKM, Chartrain L, Lasserre-Zuber P, Saintenac C. 2015. Genetics of
691 resistance to *Zymoseptoria tritici* and applications to wheat breeding. *Fungal*
692 *Genet Biol* **79**:33–41. doi:10.1016/j.fgb.2015.04.017

693 Brown NA, Bass C, Baldwin TK, Chen H, Massot F, Carion PWC, Urban M, van de
694 Meene AML, Hammond-Kosack KE. 2011. Characterisation of the *Fusarium*
695 *graminearum*-Wheat Floral Interaction. *J Pathog* **2011**:e626345.
696 doi:10.4061/2011/626345

697 Brown NA, Evans J, Mead A, Hammond-Kosack KE. 2017. A spatial temporal
698 analysis of the *Fusarium graminearum* transcriptome during symptomless and
699 symptomatic wheat infection. *Mol Plant Pathol* **18**:1295–1312.
700 doi:10.1111/mpp.12564

701 Brown NA, Urban M, van de Meene AML, Hammond-Kosack KE. 2010. The infection
702 biology of *Fusarium graminearum*: defining the pathways of spikelet to
703 spikelet colonisation in wheat ears. *Fungal Biol* **114**:555–571.
704 doi:10.1016/j.funbio.2010.04.006

705 Buchfink B, Xie C, Huson DH. 2015. Fast and sensitive protein alignment using
706 DIAMOND. *Nat Methods* **12**:59–60. doi:10.1038/nmeth.3176

707 Buerstmayr M, Steiner B, Buerstmayr H. 2020. Breeding for Fusarium head blight
708 resistance in wheat—Progress and challenges. *Plant Breed* **139**:429–454.
709 doi:10.1111/pbr.12797

710 Cai H, Yu N, Liu Y, Wei X, Guo C. 2022. Meta-analysis of fungal plant pathogen
711 *Fusarium oxysporum* infection-related gene profiles using transcriptome
712 datasets. *Front Microbiol* **13**:970477. doi:10.3389/fmicb.2022.970477

713 Cavinder B, Sikhakolli U, Fellows KM, Trail F. 2012. Sexual Development and
714 Ascospore Discharge in *Fusarium graminearum*. *J Vis Exp JoVE* 3895.
715 doi:10.3791/3895

716 Chen H, King R, Smith D, Bayon C, Ashfield T, Torriani S, Kanyuka K, Hammond-
717 Kosack K, Bieri S, Rudd J. 2023. Combined pangenomics and transcriptomics
718 reveals core and redundant virulence processes in a rapidly evolving fungal
719 plant pathogen. *BMC Biol* **21**:24. doi:10.1186/s12915-023-01520-6

720 Chen Y, Li F, Tian L, Huang M, Deng R, Li X, Chen W, Wu P, Li M, Jiang H, Wu G.
721 2017. The Phenylalanine Ammonia Lyase Gene LjPAL1 Is Involved in Plant
722 Defense Responses to Pathogens and Plays Diverse Roles in *Lotus*
723 *japonicus*-Rhizobium Symbioses. *Mol Plant Microbe Interact* **30**:739–753.
724 doi:10.1094/MPMI-04-17-0080-R

725 Cools HJ, Hammond-Kosack KE. 2013. Exploitation of genomics in fungicide
726 research: current status and future perspectives. *Mol Plant Pathol* **14**:197–
727 210. doi:10.1111/mpp.12001

728 Cooper L, Elser J, Laporte M-A, Arnaud E, Jaiswal P. 2024. Planteome 2024
729 Update: Reference Ontologies and Knowledgebase for Plant Biology. *Nucleic*
730 *Acids Res* **52**:D1548–D1555. doi:10.1093/nar/gkad1028

731 Cuzick A, Seager J, Wood V, Urban M, Rutherford K, Hammond-Kosack KE. 2023.
732 A framework for community curation of interspecies interactions literature.
733 *eLife* **12**:e84658. doi:10.7554/eLife.84658

734 Cuzick A, Urban M, Hammond-Kosack K. 2008. *Fusarium graminearum* gene
735 deletion mutants map1 and tri5 reveal similarities and differences in the
736 pathogenicity requirements to cause disease on Arabidopsis and wheat floral
737 tissue. *New Phytol* **177**:990–1000. doi:10.1111/j.1469-8137.2007.02333.x

738 Darino M, Urban M, Kaur N, Machado Wood A, Grimwade-Mann M, Smith D,
739 Beacham A, Hammond-Kosack K. 2024. Identification and functional
740 characterisation of a locus for target site integration in *Fusarium*
741 *graminearum*. *Fungal Biol Biotechnol* **11**:2. doi:10.1186/s40694-024-00171-8

742 de Chaves MA, Reginatto P, da Costa BS, de Paschoal RI, Teixeira ML, Fuentefria
743 AM. 2022. Fungicide Resistance in *Fusarium graminearum* Species Complex.
744 *Curr Microbiol* **79**:62. doi:10.1007/s00284-021-02759-4

745 Dean R, Van Kan JAL, Pretorius ZA, Hammond-Kosack KE, Di Pietro A, Spanu PD,
746 Rudd JJ, Dickman M, Kahmann R, Ellis J, Foster GD. 2012. The Top 10
747 fungal pathogens in molecular plant pathology. *Mol Plant Pathol* **13**:414–430.
748 doi:10.1111/j.1364-3703.2011.00783.x

749 Desmond OJ, Manners JM, Stephens AE, Maclean DJ, Schenk PM, Gardiner DM,
750 Munn AL, Kazan K. 2008. The Fusarium mycotoxin deoxynivalenol elicits
751 hydrogen peroxide production, programmed cell death and defence
752 responses in wheat. *Mol Plant Pathol* **9**:435–445. doi:10.1111/j.1364-
753 3703.2008.00475.x

754 Dichtl K, Samantaray S, Wagener J. 2016. Cell wall integrity signalling in human
755 pathogenic fungi. *Cell Microbiol* **18**:1228–1238. doi:10.1111/cmi.12612

756 Dilks T, Halsey K, De Vos RP, Hammond-Kosack KE, Brown NA. 2019. Non-
757 canonical fungal G-protein coupled receptors promote Fusarium head blight
758 on wheat. *PLoS Pathog* **15**:e1007666. doi:10.1371/journal.ppat.1007666

759 Duba A, Goriewa-Duba K, Wachowska U, Głowacka K, Wiwart M. 2019. The
760 Associations between Leaf Morphology, Phenylalanine Ammonia Lyase
761 Activity, Reactive Oxygen Species, and Fusarium Resistance in Selected
762 Species of Wheat with Different Ploidy Levels. *Plants* **8**:360.
763 doi:10.3390/plants8100360

764 Dyer RB, Plattner RD, Kendra DF, Brown DW. 2005. *Fusarium graminearum* TR14
765 is required for high virulence and DON production on wheat but not for DON
766 synthesis in vitro. *J Agric Food Chem* **53**:9281–9287. doi:10.1021/jf051441a

767 EFSA. 2017. Risks to human and animal health related to the presence of
768 deoxynivalenol and its acetylated and modified forms in food and feed |
769 EFSA. <https://www.efsa.europa.eu/en/efsajournal/pub/4718>

770 Estep LK, Torriani SFF, Zala M, Anderson NP, Flowers MD, McDonald BA, Mundt
771 CC, Brunner PC. 2015. Emergence and early evolution of fungicide resistance
772 in North American populations of *Zymoseptoria tritici*. *Plant Pathol* **64**:961–
773 971. doi:10.1111/ppa.12314

774 European Commission. 2022. Farm to Fork.
775 https://ec.europa.eu/commission/presscorner/detail/en/qanda_22_3694

776 European Commission. 2006. On the presence of deoxynivalenol, zearalenone,
777 ochratoxin A, T-2 and HT-2 and fumonisins in products intended for animal
778 feeding. *Off J Eur Union*, L 229/7.

779 Fones H, Gurr S. 2015. The impact of Septoria tritici Blotch disease on wheat: An EU
780 perspective. *Fungal Genet Biol* **79**:3–7. doi:10.1016/j.fgb.2015.04.004

781 Gaffoor I, Brown DW, Plattner R, Proctor RH, Qi W, Trail F. 2005. Functional
782 analysis of the polyketide synthase genes in the filamentous fungus
783 *Gibberella zeae* (anamorph *Fusarium graminearum*). *Eukaryot Cell* **4**:1926–
784 1933. doi:10.1128/EC.4.11.1926-1933.2005

785 Ghorbel M, Zribi I, Besbes M, Bouali N, Brini F. 2023. Catalase Gene Family in
786 Durum Wheat: Genome-Wide Analysis and Expression Profiling in Response
787 to Multiple Abiotic Stress Conditions. *Plants* **12**:2720.
788 doi:10.3390/plants12142720

789 Goodwin SB, M'barek SB, Dhillon B, Wittenberg AHJ, Crane CF, Hane JK, Foster
790 AJ, Van der Lee TAJ, Grimwood J, Aerts A, Antoniw J, Bailey A, Bluhm B,
791 Bowler J, Bristow J, van der Burgt A, Canto-Canché B, Churchill ACL, Conde-
792 Ferràez L, Cools HJ, Coutinho PM, Csukai M, Dehal P, De Wit P, Donzelli B,
793 van de Geest HC, van Ham RCHJ, Hammond-Kosack KE, Henrissat B, Kilian
794 A, Kobayashi AK, Koopmann E, Kourmpetis Y, Kuzniar A, Lindquist E,
795 Lombard V, Maliepaard C, Martins N, Mehrabi R, Nap JPH, Ponomarenko A,
796 Rudd JJ, Salamov A, Schmutz J, Schouten HJ, Shapiro H, Stergiopoulos I,
797 Torriani SFF, Tu H, de Vries RP, Waalwijk C, Ware SB, Wiebenga A, Zwiars
798 L-H, Oliver RP, Grigoriev IV, Kema GHJ. 2011. Finished genome of the fungal
799 wheat pathogen *Mycosphaerella graminicola* reveals dispensome structure,
800 chromosome plasticity, and stealth pathogenesis. *PLoS Genet* **7**:e1002070.
801 doi:10.1371/journal.pgen.1002070

802 Götz S, García-Gómez JM, Terol J, Williams TD, Nagaraj SH, Nueda MJ, Robles M,
803 Talón M, Dopazo J, Conesa A. 2008. High-throughput functional annotation

804 and data mining with the Blast2GO suite. *Nucleic Acids Res* **36**:3420–3435.
805 doi:10.1093/nar/gkn176

806 Hahlbrock K, Scheel D. 1989. Physiology and Molecular Biology of Phenylpropanoid
807 Metabolism. *Annu Rev Plant Physiol Plant Mol Biol* **40**:347–369.
808 doi:10.1146/annurev.pp.40.060189.002023

809 Hassani-Pak K, Singh A, Brandizi M, Hearnshaw J, Parsons JD, Amberkar S,
810 Phillips AL, Doonan JH, Rawlings C. 2021. KnetMiner: a comprehensive
811 approach for supporting evidence-based gene discovery and complex trait
812 analysis across species. *Plant Biotechnol J* **19**:1670–1678.
813 doi:10.1111/pbi.13583

814 Hill R, Buggs RJA, Vu DT, Gaya E. 2022. Lifestyle Transitions in Fusarioid Fungi are
815 Frequent and Lack Clear Genomic Signatures. *Mol Biol Evol* **39**.
816 doi:10.1093/molbev/msac085

817 Hou Z, Xue C, Peng Y, Katan T, Kistler HC, Xu J-R. 2002. A mitogen-activated
818 protein kinase gene (MGV1) in *Fusarium graminearum* is required for female
819 fertility, heterokaryon formation, and plant infection. *Mol Plant-Microbe*
820 *Interact MPMI* **15**:1119–1127. doi:10.1094/MPMI.2002.15.11.1119

821 Huerta-Cepas J, Szklarczyk D, Heller D, Hernández-Plaza A, Forslund SK, Cook H,
822 Mende DR, Letunic I, Rattei T, Jensen LJ, von Mering C, Bork P. 2019.
823 eggNOG 5.0: a hierarchical, functionally and phylogenetically annotated
824 orthology resource based on 5090 organisms and 2502 viruses. *Nucleic Acids*
825 *Res* **47**:D309–D314. doi:10.1093/nar/gky1085

826 Jansen C, von Wettstein D, Schäfer W, Kogel K-H, Felk A, Maier FJ. 2005. Infection
827 patterns in barley and wheat spikes inoculated with wild-type and trichodiene
828 synthase gene disrupted *Fusarium graminearum*. *Proc Natl Acad Sci*
829 **102**:16892–16897. doi:10.1073/pnas.0508467102

830 Jeger M, Beresford R, Bock C, Brown N, Fox A, Newton A, Vicent A, Xu X, Yuen J.
831 2021. Global challenges facing plant pathology: multidisciplinary approaches
832 to meet the food security and environmental challenges in the mid-twenty-first
833 century. *CABI Agric Biosci* **2**:20. doi:10.1186/s43170-021-00042-x

834 Jenczmionka NJ, Maier FJ, Löscher AP, Schäfer W. 2003. Mating, conidiation and
835 pathogenicity of *Fusarium graminearum*, the main causal agent of the head-
836 blight disease of wheat, are regulated by the MAP kinase gpmk1. *Curr Genet*
837 **43**:87–95. doi:10.1007/s00294-003-0379-2

838 John E, Singh KB, Oliver RP, Tan K-C. 2021. Transcription factor control of virulence
839 in phytopathogenic fungi. *Mol Plant Pathol* **22**:858–881.
840 doi:10.1111/mpp.13056

841 Johns LE, Bebbler DP, Gurr SJ, Brown NA. 2022. Emerging health threat and cost of
842 *Fusarium* mycotoxins in European wheat. *Nat Food* **3**:1014–1019.
843 doi:10.1038/s43016-022-00655-z

844 Kanja C, Wood AKM, Baggaley L, Walker C, Hammond-Kosack KE. 2021. Cereal-
845 *Fusarium* interactions: Improved fundamental insights into *Fusarium*
846 pathogenomics and cereal host resistance reveals new ways to achieve
847 durable disease control. Achieving Durable Disease Resistance in Cereals.
848 Burleigh Dodds Science Publishing.

849 Kema GHJ, Yu D, Frits H. J R, Michael W. S, Robert P. B. 1996. Histology of the
850 Pathogenesis of *Mycosphaerella graminicola* in Wheat. *Phytopathology*
851 **86**:777–786.

852 Keon J, Antoniw J, Carzaniga R, Deller S, Ward JL, Baker JM, Beale MH,
853 Hammond-Kosack K, Rudd JJ. 2007. Transcriptional adaptation of

854 *Mycosphaerella graminicola* to programmed cell death (PCD) of its
855 susceptible wheat host. *Mol Plant-Microbe Interact MPMI* **20**:178–193.
856 doi:10.1094/MPMI-20-2-0178

857 Kim DS, Hwang BK. 2014. An important role of the pepper phenylalanine ammonia-
858 lyase gene (PAL1) in salicylic acid-dependent signalling of the defence
859 response to microbial pathogens. *J Exp Bot* **65**:2295–2306.
860 doi:10.1093/jxb/eru109

861 Kimura M, Tokai T, Takahashi-Ando N, Ohsato S, Fujimura M. 2007. Molecular and
862 genetic studies of fusarium trichothecene biosynthesis: pathways, genes, and
863 evolution. *Biosci Biotechnol Biochem* **71**:2105–2123. doi:10.1271/bbb.70183

864 King R, Urban M, Hammond-Kosack KE. 2017a. Annotation of *Fusarium*
865 *graminearum* (PH-1) Version 5.0. *Genome Announc* **5**:e01479-16.
866 doi:10.1128/genomeA.01479-16

867 King R, Urban M, Lauder RP, Hawkins N, Evans M, Plummer A, Halsey K,
868 Lovegrove A, Hammond-Kosack K, Rudd JJ. 2017b. A conserved fungal
869 glycosyltransferase facilitates pathogenesis of plants by enabling hyphal
870 growth on solid surfaces. *PLoS Pathog* **13**:e1006672.
871 doi:10.1371/journal.ppat.1006672

872 Kugler KG, Siegwart G, Nussbaumer T, Ametz C, Spannagl M, Steiner B, Lemmens
873 M, Mayer KF, Buerstmayr H, Schweiger W. 2013. Quantitative trait loci-
874 dependent analysis of a gene co-expression network associated with
875 *Fusarium* head blight resistance in bread wheat (*Triticum aestivum* L.). *BMC*
876 *Genomics* **14**:728. doi:10.1186/1471-2164-14-728

877 Langfelder P, Horvath S. 2008. WGCNA: an R package for weighted correlation
878 network analysis. *BMC Bioinformatics* **9**:559. doi:10.1186/1471-2105-9-559

879 Langfelder P, Luo R, Oldham MC, Horvath S. 2011. Is My Network Module
880 Preserved and Reproducible? *PLOS Comput Biol* **7**:e1001057.
881 doi:10.1371/journal.pcbi.1001057

882 Latham RL, Boyle JT, Barbano A, Loveman WG, Brown NA. 2023. Diverse
883 mycotoxin threats to safe food and feed cereals. *Essays Biochem* **67**:797–
884 809. doi:10.1042/EBC20220221

885 Letunic I, Bork P. 2024. Interactive Tree of Life (iTOL) v6: recent updates to the
886 phylogenetic tree display and annotation tool. *Nucleic Acids Res*.
887 doi:10.1093/nar/gkae268

888 Li D, Walker E, Francki M. 2021. Genes Associated with Foliar Resistance to
889 *Septoria Nodorum* Blotch of Hexaploid Wheat (*Triticum aestivum* L.). *Int J Mol*
890 *Sci* **22**:5580. doi:10.3390/ijms22115580

891 Li L, He Z, Pandey GK, Tsuchiya T, Luan S. 2002. Functional Cloning and
892 Characterization of a Plant Efflux Carrier for Multidrug and Heavy Metal
893 Detoxification. *J Biol Chem* **277**:5360–5368. doi:10.1074/jbc.M108777200

894 Liu Z, Zhu Z, Huang Y, Nong S, Jiang M, Yi S, Xie D, Hu H. 2023. Identification of
895 gene modules and hub genes associated with *Colletotrichum siamense*
896 infection in mango using weighted gene co-expression network analysis. *BMC*
897 *Genomics* **24**:710. doi:10.1186/s12864-023-09811-6

898 Love MI, Huber W, Anders S. 2014. Moderated estimation of fold change and
899 dispersion for RNA-seq data with DESeq2. *Genome Biol* **15**:550.
900 doi:10.1186/s13059-014-0550-8

901 Lu S, Faris JD. 2019. *Fusarium graminearum* KP4-like proteins possess root growth-
902 inhibiting activity against wheat and potentially contribute to fungal virulence in
903 seedling rot. *Fungal Genet Biol* **123**:1–13. doi:10.1016/j.fgb.2018.11.002

904 Lucas JA, Hawkins NJ, Fraaije BA. 2015. The evolution of fungicide resistance. *Adv*
905 *Appl Microbiol* **90**:29–92. doi:10.1016/bs.aambs.2014.09.001

906 Machado AK, Brown NA, Urban M, Kanyuka K, Hammond-Kosack KE. 2018. RNAi
907 as an emerging approach to control *Fusarium* head blight disease and
908 mycotoxin contamination in cereals. *Pest Manag Sci* **74**:790–799.
909 doi:10.1002/ps.4748

910 Maher EA, Bate NJ, Ni W, Elkind Y, Dixon RA, Lamb CJ. 1994. Increased disease
911 susceptibility of transgenic tobacco plants with suppressed levels of
912 preformed phenylpropanoid products. *Proc Natl Acad Sci* **91**:7802–7806.
913 doi:10.1073/pnas.91.16.7802

914 Mann CWG, Sawyer A, Gardiner DM, Mitter N, Carroll BJ, Eamens AL. 2023. RNA-
915 Based Control of Fungal Pathogens in Plants. *Int J Mol Sci* **24**:12391.
916 doi:10.3390/ijms241512391

917 Martin H, Dagkessamanskaia A, Satchanska G, Dallies N, François J. 1999. KNR4,
918 a suppressor of *Saccharomyces cerevisiae* cwh mutants, is involved in the
919 transcriptional control of chitin synthase genes. *Microbiol Read Engl* **145 (Pt**
920 **1)**:249–258. doi:10.1099/13500872-145-1-249

921 Martin-Yken H, Dagkessamanskaia A, Basmaji F, Lagorce A, Francois J. 2003. The
922 interaction of Slr2 MAP kinase with Knr4 is necessary for signalling through
923 the cell wall integrity pathway in *Saccharomyces cerevisiae*. *Mol Microbiol*
924 **49**:23–35. doi:10.1046/j.1365-2958.2003.03541.x

925 Mateus ID, Masclaux FG, Aletti C, Rojas EC, Savary R, Dupuis C, Sanders IR. 2019.
926 Dual RNA-seq reveals large-scale non-conserved genotype x genotype-
927 specific genetic reprogramming and molecular crosstalk in the mycorrhizal
928 symbiosis. *ISME J* **13**:1226–1238. doi:10.1038/s41396-018-0342-3

929 McDonald MC, Renkin M, Spackman M, Orchard B, Croll D, Solomon PS, Milgate A.
930 2019. Rapid Parallel Evolution of Azole Fungicide Resistance in Australian
931 Populations of the Wheat Pathogen *Zymoseptoria tritici*. *Appl Environ*
932 *Microbiol* **85**:e01908-18. doi:10.1128/AEM.01908-18

933 Motteram J, Lovegrove A, Pirie E, Marsh J, Devonshire J, van de Meene A,
934 Hammond-Kosack K, Rudd JJ. 2011. Aberrant protein N-glycosylation
935 impacts upon infection-related growth transitions of the haploid plant-
936 pathogenic fungus *Mycosphaerella graminicola*. *Mol Microbiol* **81**:415–433.
937 doi:10.1111/j.1365-2958.2011.07701.x

938 Nelson R. 2020. International Plant Pathology: Past and Future Contributions to
939 Global Food Security. *Phytopathology* **110**:245–253. doi:10.1094/PHYTO-08-
940 19-0300-IA

941 Nguyen T, Kröger C, Bönninghausen J, Schäfer W, Bormann J. 2013. The ATF/CREB
942 Transcription Factor Atf1 Is Essential for Full Virulence, Deoxynivalenol
943 Production, and Stress Tolerance in the Cereal Pathogen *Fusarium*
944 *graminearum*. *Mol Plant-Microbe Interact MPMI* **26**. doi:10.1094/MPMI-04-13-
945 0125-R

946 O'Donnell K, Kistler HC, Tacke BK, Casper HH. 2000. Gene genealogies reveal
947 global phylogeographic structure and reproductive isolation among lineages of
948 *Fusarium graminearum*, the fungus causing wheat scab. *Proc Natl Acad Sci*
949 **97**:7905–7910. doi:10.1073/pnas.130193297

950 Oldham M. 2014. M. Transcriptomics: from differential expression to coexpression.
951 The OMICs: Applications in Neuroscience. Oxford University Press, UK.

952 Pan Y, Liu Z, Rocheleau H, Fauteux F, Wang Y, McCartney C, Ouellet T. 2018.
953 Transcriptome dynamics associated with resistance and susceptibility against

954 fusarium head blight in four wheat genotypes. *BMC Genomics* **19**:642.
955 doi:10.1186/s12864-018-5012-3

956 Park J, Lee H-H, Moon H, Lee N, Kim S, Kim J-E, Lee Y, Min K, Kim H, Choi GJ,
957 Lee Y-W, Seo Y-S, Son H. 2023. A combined transcriptomic and physiological
958 approach to understanding the adaptive mechanisms to cope with oxidative
959 stress in *Fusarium graminearum*. *Microbiol Spectr* **11**:e01485-23.
960 doi:10.1128/spectrum.01485-23

961 Perincherry L, Lalak-Kańczugowska J, Stępień Ł. 2019. Fusarium-Produced
962 Mycotoxins in Plant-Pathogen Interactions. *Toxins* **11**:664.
963 doi:10.3390/toxins11110664

964 Plissonneau C, Hartmann FE, Croll D. 2018. Pangenome analyses of the wheat
965 pathogen *Zymoseptoria tritici* reveal the structural basis of a highly plastic
966 eukaryotic genome. *BMC Biol* **16**:5. doi:10.1186/s12915-017-0457-4

967 Ramarosan M-L, Koutouan C, Helesbeux J-J, Le Clerc V, Hamama L, Geoffriau E,
968 Briard M. 2022. Role of Phenylpropanoids and Flavonoids in Plant Resistance
969 to Pests and Diseases. *Molecules* **27**:8371. doi:10.3390/molecules27238371

970 Robinson MD, McCarthy DJ, Smyth GK. 2010. edgeR: a Bioconductor package for
971 differential expression analysis of digital gene expression data. *Bioinforma*
972 *Oxf Engl* **26**:139–140. doi:10.1093/bioinformatics/btp616

973 Rudd JJ, Kanyuka K, Hassani-Pak K, Derbyshire M, Andongabo A, Devonshire J,
974 Lysenko A, Saqi M, Desai NM, Powers SJ, Hooper J, Ambroso L, Bharti A,
975 Farmer A, Hammond-Kosack KE, Dietrich RA, Courbot M. 2015.
976 Transcriptome and Metabolite Profiling of the Infection Cycle of *Zymoseptoria*
977 *tritici* on Wheat Reveals a Biphasic Interaction with Plant Immunity Involving
978 Differential Pathogen Chromosomal Contributions and a Variation on the
979 Hemibiotrophic Lifestyle Definition. *Plant Physiol* **167**:1158–1185.
980 doi:10.1104/pp.114.255927

981 Saldivar SOS. 2016. Cereals: Dietary Importance In: Caballero B, Finglas PM,
982 Toldrá F, editors. *Encyclopedia of Food and Health*. Oxford: Academic Press.
983 pp. 703–711. doi:10.1016/B978-0-12-384947-2.00130-6

984 Savary S, Willocquet L, Pethybridge SJ, Esker P, McRoberts N, Nelson A. 2019. The
985 global burden of pathogens and pests on major food crops. *Nat Ecol Evol*
986 **3**:430–439. doi:10.1038/s41559-018-0793-y

987 Schneider CA, Rasband WS, Eliceiri KW. 2012. NIH Image to ImageJ: 25 years of
988 image analysis. *Nat Methods* **9**:671–675. doi:10.1038/nmeth.2089

989 Sertsuvalkul N, DeMell A, Dinesh-Kumar SP. 2022. The complex roles of autophagy
990 in plant immunity. *FEBS Lett* **596**:2163–2171. doi:10.1002/1873-3468.14356

991 Shewry PR, Hey SJ. 2015. The contribution of wheat to human diet and health. *Food*
992 *Energy Secur* **4**:178–202. doi:10.1002/fes3.64

993 Shin Y-K, Kim D-W, Lee S-W, Lee M-J, Gi Baek S, Lee T, Yun S-H. 2022. Functional
994 roles of all five putative hydrophobin genes in growth, development, and
995 secondary metabolism in *Fusarium graminearum*. *Fungal Genet Biol*
996 **160**:103683. doi:10.1016/j.fgb.2022.103683

997 Sieber CMK, Lee W, Wong P, Münsterkötter M, Mewes H-W, Schmeitzl C, Varga E,
998 Berthiller F, Adam G, Güldener U. 2014. The *Fusarium graminearum* Genome
999 Reveals More Secondary Metabolite Gene Clusters and Hints of Horizontal
1000 Gene Transfer. *PLOS ONE* **9**:e110311. doi:10.1371/journal.pone.0110311

1001 Son H, Seo Y-S, Min K, Park AR, Lee J, Jin J-M, Lin Y, Cao P, Hong S-Y, Kim E-K,
1002 Lee S-H, Cho A, Lee S, Kim M-G, Kim Y, Kim J-E, Kim J-C, Choi GJ, Yun S-
1003 H, Lim JY, Kim M, Lee Y-H, Choi Y-D, Lee Y-W. 2011. A Phenome-Based

1004 Functional Analysis of Transcription Factors in the Cereal Head Blight
1005 Fungus, *Fusarium graminearum*. *PLoS Pathog* **7**:e1002310.
1006 doi:10.1371/journal.ppat.1002310

1007 Sperschneider J, Dodds PN. 2022. EffectorP 3.0: Prediction of Apoplastic and
1008 Cytoplasmic Effectors in Fungi and Oomycetes. *Mol Plant-Microbe Interact*
1009 *MPMI* **35**:146–156. doi:10.1094/MPMI-08-21-0201-R

1010 Steinberg G. 2015. Cell biology of *Zymoseptoria tritici*: Pathogen cell organization
1011 and wheat infection. *Fungal Genet Biol* **79**:17–23.
1012 doi:10.1016/j.fgb.2015.04.002

1013 Teufel F, Almagro Armenteros JJ, Johansen AR, Gíslason MH, Pihl SI, Tsigos KD,
1014 Winther O, Brunak S, von Heijne G, Nielsen H. 2022. SignalP 6.0 predicts all
1015 five types of signal peptides using protein language models. *Nat Biotechnol*
1016 **40**:1023–1025. doi:10.1038/s41587-021-01156-3

1017 Tonnessen BW, Manosalva P, Lang JM, Baraoidan M, Bordeos A, Mauleon R, Oard
1018 J, Hulbert S, Leung H, Leach JE. 2015. Rice phenylalanine ammonia-lyase
1019 gene OsPAL4 is associated with broad spectrum disease resistance. *Plant*
1020 *Mol Biol* **87**:273–286. doi:10.1007/s11103-014-0275-9

1021 Torriani SFF, Melichar JPE, Mills C, Pain N, Sierotzki H, Courbot M. 2015.
1022 *Zymoseptoria tritici*: A major threat to wheat production, integrated
1023 approaches to control. *Fungal Genet Biol* **79**:8–12.
1024 doi:10.1016/j.fgb.2015.04.010

1025 Urban M, Cuzick A, Seager J, Wood V, Rutherford K, Venkatesh SY, Sahu J, Iyer
1026 SV, Khamari L, De Silva N, Martinez MC, Pedro H, Yates AD, Hammond-
1027 Kosack KE. 2022. PHI-base in 2022: a multi-species phenotype database for
1028 Pathogen–Host Interactions. *Nucleic Acids Res* **50**:D837–D847.
1029 doi:10.1093/nar/gkab1037

1030 Urban M, Mott E, Farley T, Hammond-Kosack K. 2003. The *Fusarium graminearum*
1031 MAP1 gene is essential for pathogenicity and development of perithecia. *Mol*
1032 *Plant Pathol* **4**:347–359. doi:10.1046/j.1364-3703.2003.00183.x

1033 Vicente I, Quaratiello G, Baroncelli R, Vannacci G, Sarrocco S. 2022. Insights on
1034 KP4 Killer Toxin-like Proteins of *Fusarium* Species in Interspecific
1035 Interactions. *J Fungi* **8**:968. doi:10.3390/jof8090968

1036 Walsh CJ, Batt J, Herridge MS, Mathur S, Bader GD, Hu P, dos Santos CC. 2016.
1037 Transcriptomic analysis reveals abnormal muscle repair and remodeling in
1038 survivors of critical illness with sustained weakness. *Sci Rep* **6**:29334.
1039 doi:10.1038/srep29334

1040 Wang C, Zhang S, Hou R, Zhao Z, Zheng Q, Xu Q, Zheng D, Wang G, Liu H, Gao X,
1041 Ma J-W, Kistler HC, Kang Z, Xu J-R. 2011. Functional analysis of the kinome
1042 of the wheat scab fungus *Fusarium graminearum*. *PLoS Pathog* **7**:e1002460.
1043 doi:10.1371/journal.ppat.1002460

1044 Xu M, Wang Q, Wang G, Zhang X, Liu H, Jiang C. 2022. Combatting *Fusarium* head
1045 blight: advances in molecular interactions between *Fusarium graminearum*
1046 and wheat. *Phytopathol Res* **4**:37. doi:10.1186/s42483-022-00142-0

1047 Yan X, Tang B, Ryder LS, MacLean D, Were VM, Eseola AB, Cruz-Mireles N, Ma W,
1048 Foster AJ, Osés-Ruiz M, Talbot NJ. 2023. The transcriptional landscape of
1049 plant infection by the rice blast fungus *Magnaporthe oryzae* reveals distinct
1050 families of temporally co-regulated and structurally conserved effectors. *Plant*
1051 *Cell* **35**:1360–1385. doi:10.1093/plcell/koad036

1052 Yu J-H, Hamari Z, Han K-H, Seo J-A, Reyes-Domínguez Y, Scazzocchio C. 2004.
1053 Double-joint PCR: a PCR-based molecular tool for gene manipulations in

- 1054 filamentous fungi. *Fungal Genet Biol FG B* **41**:973–981.
1055 doi:10.1016/j.fgb.2004.08.001
- 1056 Yun Y, Liu Z, Zhang J, Shim W-B, Chen Y, Ma Z. 2014. The MAPKK FgMkk1 of
1057 *Fusarium graminearum* regulates vegetative differentiation, multiple stress
1058 response, and virulence via the cell wall integrity and high-osmolarity glycerol
1059 signaling pathways. *Environ Microbiol* **16**:2023–2037. doi:10.1111/1462-
1060 2920.12334
- 1061 Zhang B, Horvath S. 2005. A general framework for weighted gene co-expression
1062 network analysis. *Stat Appl Genet Mol Biol* **4**:Article17. doi:10.2202/1544-
1063 6115.1128
- 1064 Zhang L, Zhou X, Li P, Wang Y, Hu Q, Shang Y, Chen Y, Zhu X, Feng H, Zhang C.
1065 2022. Transcriptome Profile of *Fusarium graminearum* Treated by Putrescine.
1066 *J Fungi* **9**:60. doi:10.3390/jof9010060
- 1067 Zhang Yu, Chen W, Shao W, Tan S, Shi D, Ma H, Chen C. 2022. FaSmi1 Is
1068 Essential for the Vegetative Development, Asexual Reproduction, DON
1069 Production and Virulence of *Fusarium asiaticum*. *J Fungi* **8**:1189.
1070 doi:10.3390/jof8111189
- 1071 Zhang Y, Dai Y, Huang Y, Wang K, Lu P, Xu H, Xu J-R, Liu H. 2020. The SR-protein
1072 FgSrp2 regulates vegetative growth, sexual reproduction and pre-mRNA
1073 processing by interacting with FgSrp1 in *Fusarium graminearum*. *Curr Genet*
1074 **66**:607–619. doi:10.1007/s00294-020-01054-2
- 1075 Zhang Yan, Zheng L, Yun L, Ji L, Li G, Ji M, Shi Y, Zheng X. 2022. Catalase (CAT)
1076 Gene Family in Wheat (*Triticum aestivum* L.): Evolution, Expression Pattern
1077 and Function Analysis. *Int J Mol Sci* **23**:542. doi:10.3390/ijms23010542
- 1078 Zheng D, Zhang S, Zhou X, Wang C, Xiang P, Zheng Q, Xu J-R. 2012. The FgHOG1
1079 Pathway Regulates Hyphal Growth, Stress Responses, and Plant Infection in
1080 *Fusarium graminearum*. *PLOS ONE* **7**:e49495.
1081 doi:10.1371/journal.pone.0049495
- 1082 Zhu T, Wang L, Rimbart H, Rodriguez JC, Deal KR, De Oliveira R, Choulet F,
1083 Keeble-Gagnère G, Tibbits J, Rogers J, Eversole K, Appels R, Gu YQ,
1084 Mascher M, Dvorak J, Luo M-C. 2021. Optical maps refine the bread wheat
1085 *Triticum aestivum* cv. Chinese Spring genome assembly. *Plant J* **107**:303–
1086 314. doi:10.1111/tbj.15289

1087

1088 Funding

- 1089 E.K and V.A are supported by the BBSRC-funded South West Biosciences Doctoral Training
1090 Partnership (BB/T008741/1). K.H.K and M.U are supported by the Biotechnology and
1091 Biological Sciences Research Council (BBSRC) Institute Strategic Programme (ISP) Grants,
1092 Designing Future Wheat (BBS/E/C/000I0250) and Delivering Sustainable Wheat
1093 (BB/X011003/1 and BBS/E/RH/230001B) and the BBSRC grants (BB/X012131/1 and
1094 BB/W007134/1). N.A.B was supported by the BBSRC Future Leader Fellowship

1095 BB/N011686/1. J.R and C.B are funded by the BBSRC ISPs Designing Future Wheat
1096 (BBS/E/C/00010250), Delivering Sustainable Wheat (BB/X011003/1 and
1097 BBS/E/RH/230001B), and Growing Health (BB/X010953). R.A was supported by a
1098 BBSRC/EPSRC Interface Innovation Fellowship (EP/S001352/1).

1099 **Author's contributions**

1100 E.K conducted the experiments and wrote the manuscript. N.A.B, M.U, and K.H.K
1101 provided project oversight, experimental design and manuscript planning,
1102 development, and revisions. R.A helped with experimental design and data analysis.
1103 C.B and J.R generated the *ZtKnr4* mutant and completed associated
1104 characterisation experiments. A.M.U embedded, sectioned, and imaged samples for
1105 TEM analysis. V.A undertook the resin embedding, sectioning, and imaging.

1106

1107 **Competing interests**

1108 No competing interests declared.

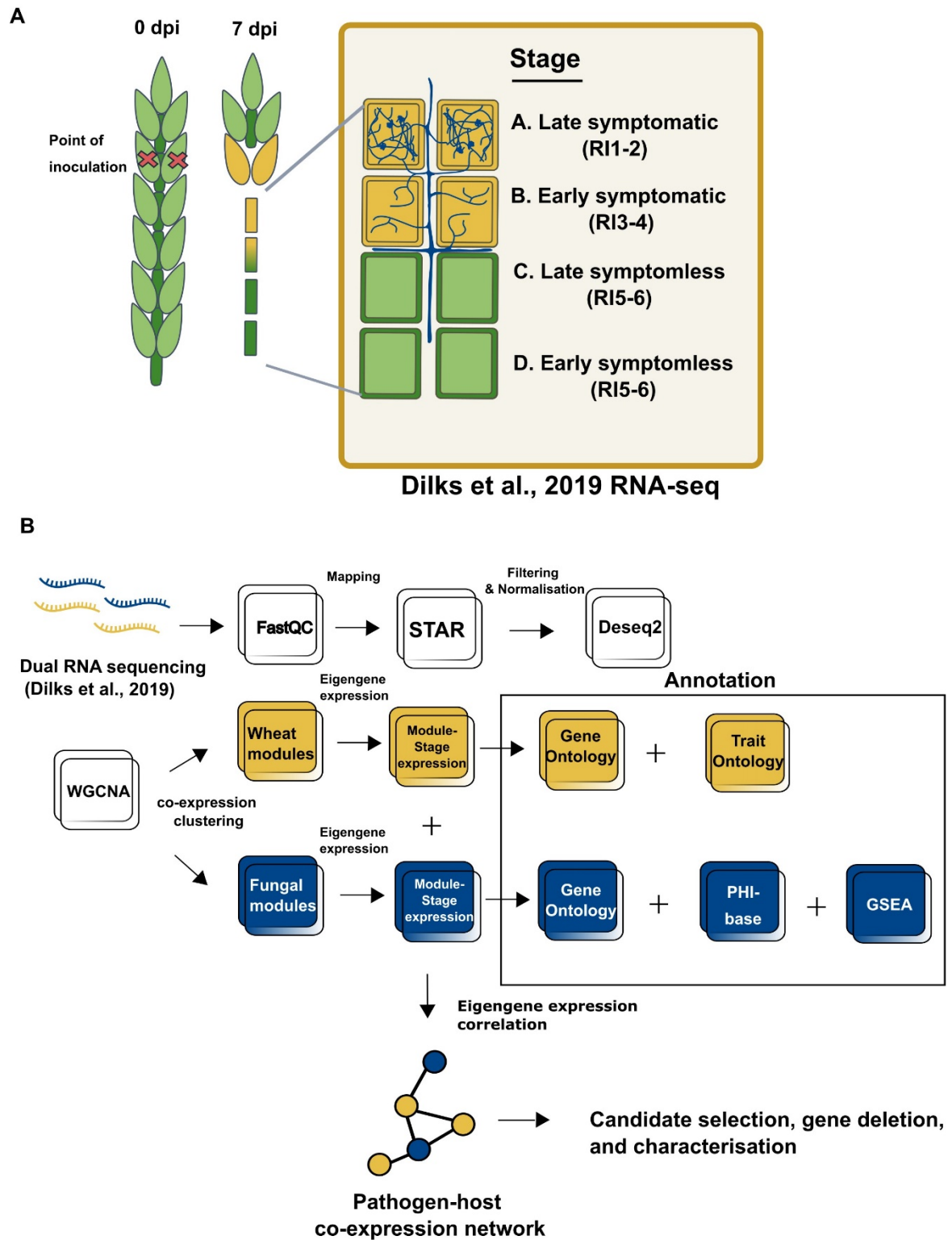
1109 **Tables and Figures**

1110

1111 **Table 1. Function of correlated expression between wheat and fungal modules.** This table illustrates the relationship between wheat and
 1112 fungal gene expression at different stages of infection, detailing the associated functions and key fungal genes involved.

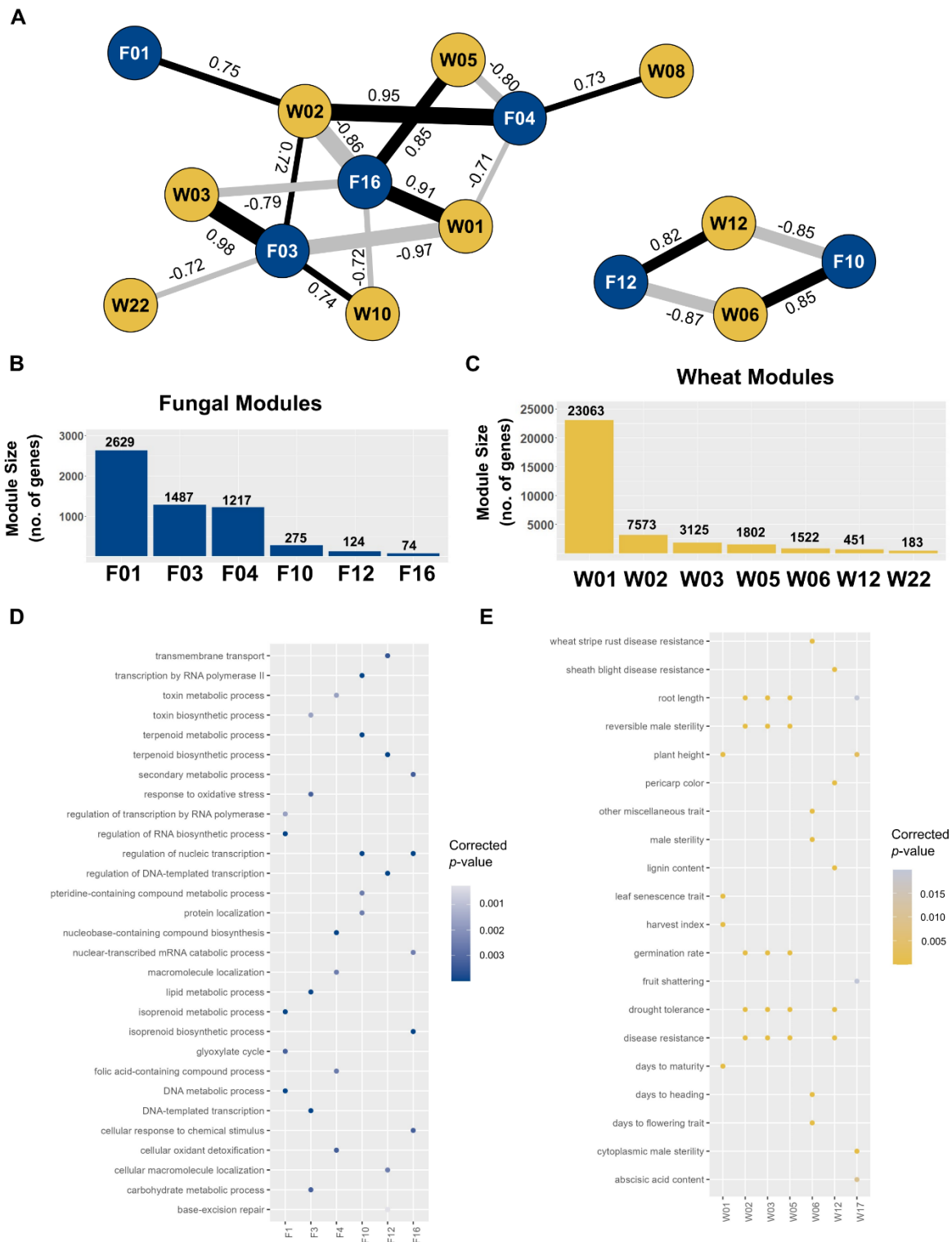
Expression Stages	Wheat Module	Predicted function	Correlated Fungal Module	Key Fungal Genes	Fungal Gene Functions	References
Early symptomless stage of infection	W01	Maintenance genes (photosynthesis, RNA modification) and early defence response.	F16	<i>FgNPC1</i>	Regulation of membrane trafficking and sterol metabolism, which are essential for maintaining cellular integrity and function during the infection stages.	Breakspear et al. 2011
				<i>Gzc2h045</i>	Msn2 C2H2 transcription factor, associated with virulence and coordination of adaptation to environmental stressors including heat, osmotic, and oxidative stress.	Son et al., 2011; John et al., 2021
	W05	Disease resistance genes, including reactive oxygen species genes associated with programmed cell death response to restrict pathogen spread.		<i>GzCon7</i>	Msn2 C2H2 transcription factor, associated with virulence and regulation of cell wall biosynthesis.	Son et al., 2011; John et al., 2021
				<i>FgSrp2</i>	Pre-mRNA processing, alternative splicing, and virulence	Zhang et al., 2020

Early symptomless and late symptomatic stages of infection	W06	Enriched in protein catabolism and autophagy, involved in immune signalling, programmed cell death, and necrotrophic damage control.	F10	<i>KP4L-1, KP4L-2, KP4L-3</i>	Necessary for virulence, provide competitive advantage during new niche occupation, essential for intraspecific interactions at high fungal density	Lu and Faris, 2019; Vicente et al., 2022
				<i>FgOS-2, FgAtf-1</i>	Regulation of secondary metabolite production, sexual reproduction, and stress tolerance	Nguyen et al., 2013
				<i>FgHyd3, FgHyd5</i>	Attachment to hydrophobic surfaces, production of aerial mycelia	Shin et al., 2022
Late symptomless to early symptomatic	W12	Detoxification, response to toxic substances, and defence response.	F12	<i>TRI</i> genes (<i>TRI3, TRI4, TRI11, TRI12, TRI14</i>)	Production of DON mycotoxin needed for virulence.	Dyer et al., 2005; Kimura et al., 2007



1118 and symptomless (green) stages of *Fusarium graminearum* infection of wheat spikes
1119 denoted as stages A through D, corresponding to tissue samples collected for generating the
1120 RNA-seq data published in Dilks et al. 2019. *F. graminearum* hyphae growing in either the
1121 apoplast or inside the wheat cells are depicted in blue. **B.** Summary outlining the
1122 bioinformatics pipeline used for processing raw reads and constructing the dual RNA-seq
1123 network. The dual RNA-seq reads were initially processed together (processes depicted as
1124 white squares) before being separated to generate two distinct weighted gene co-expression
1125 networks. The bioinformatic pipelines are annotated accordingly, with yellow indicating the
1126 wheat reads-only pipeline and blue indicating the fungal reads-only pipeline. Annotation
1127 includes Gene Ontology terms (GO), Trait Ontology terms (TO), unique Gene Set
1128 Enrichment Analysis (GSEA), and PHI-base phenotypes. The modules from the two
1129 separate networks are then correlated to each other by their eigengene values to form the
1130 dual co-expression network.

1131



1132

1133

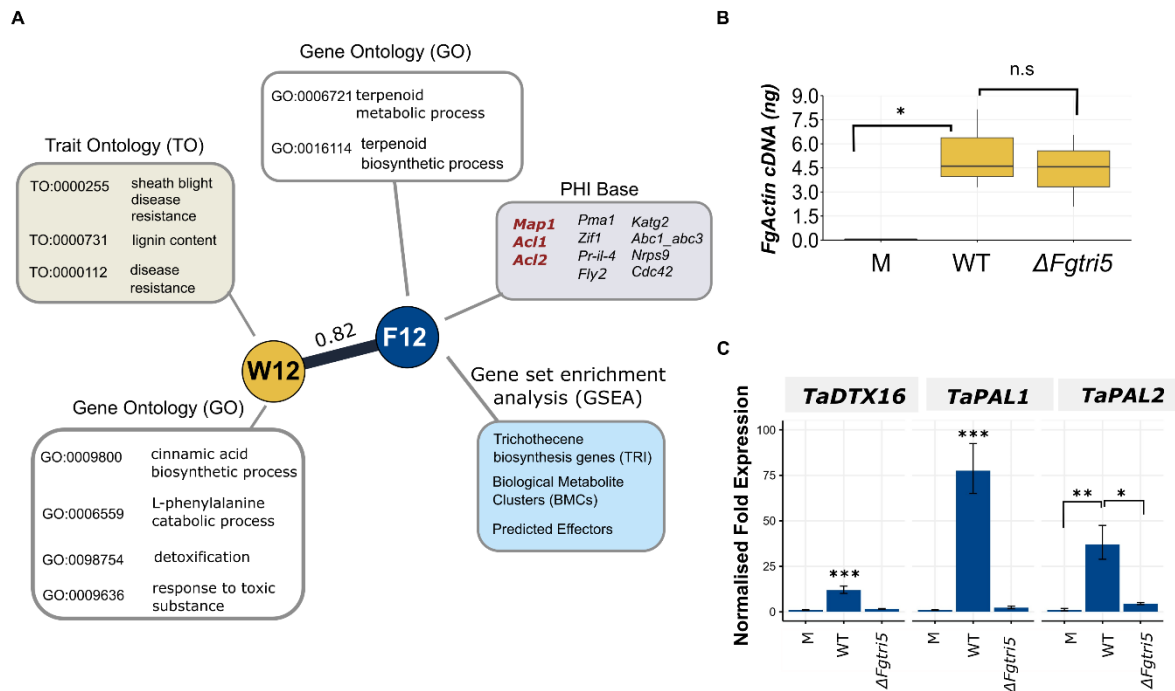
1134 **Figure 2. Dual Fungal-Wheat co-expression network. A.** Network summarising significant

1135 co-expression patterns ($p \geq 0.001$) between fungal modules (blue nodes) and wheat

1136 modules (yellow nodes). Positive correlations are depicted as black edges, while negative

1137 correlations are shown as grey edges. R-squared values are indicated next to edges, with
1138 edge width corresponding to the value. **B. Fungal modules sizes. C. Wheat module sizes**
1139 **(Supplementary File S1). D. Fungal module enrichment.** Significant ($p \leq 0.05$) Biological
1140 Processes (BP) Gene Ontology (GO) enrichment results for all fungal modules in the
1141 network. Higher significance is indicated by darker blues. **E. Wheat module enrichment.**
1142 Significant Plant Trait Ontology (TO) enrichment results ($p \leq 0.05$) for all wheat modules in
1143 the network. Higher significance is indicated by brighter yellows.

1144



1145

1146 **Figure 3. Validation of correlation between the trichothecene mycotoxin biosynthesis**

1147 **gene enriched module (F12) and the detoxification gene enriched module (W12). A.**

1148 Modules F12 (N = 124) and W12 (N = 451) depicted with significant enrichment annotations

1149 and genes with known phenotypes from PHI-base. Three genes listed in red in the PHI-base

1150 annotation (grey box) exhibit a loss of pathogenicity phenotype, while the remaining genes

1151 display a reduced virulence phenotype when individually deleted in *F. graminearum*. **B.**

1152 Equal levels of fungal burden were observed in tissue samples ($p > 0.05$). Absolute quantity

1153 of actin cDNA in Mock, $\Delta Fgtri5$, and wild-type (WT)-recovered RI1-2 tissue sampled at 3 dpi

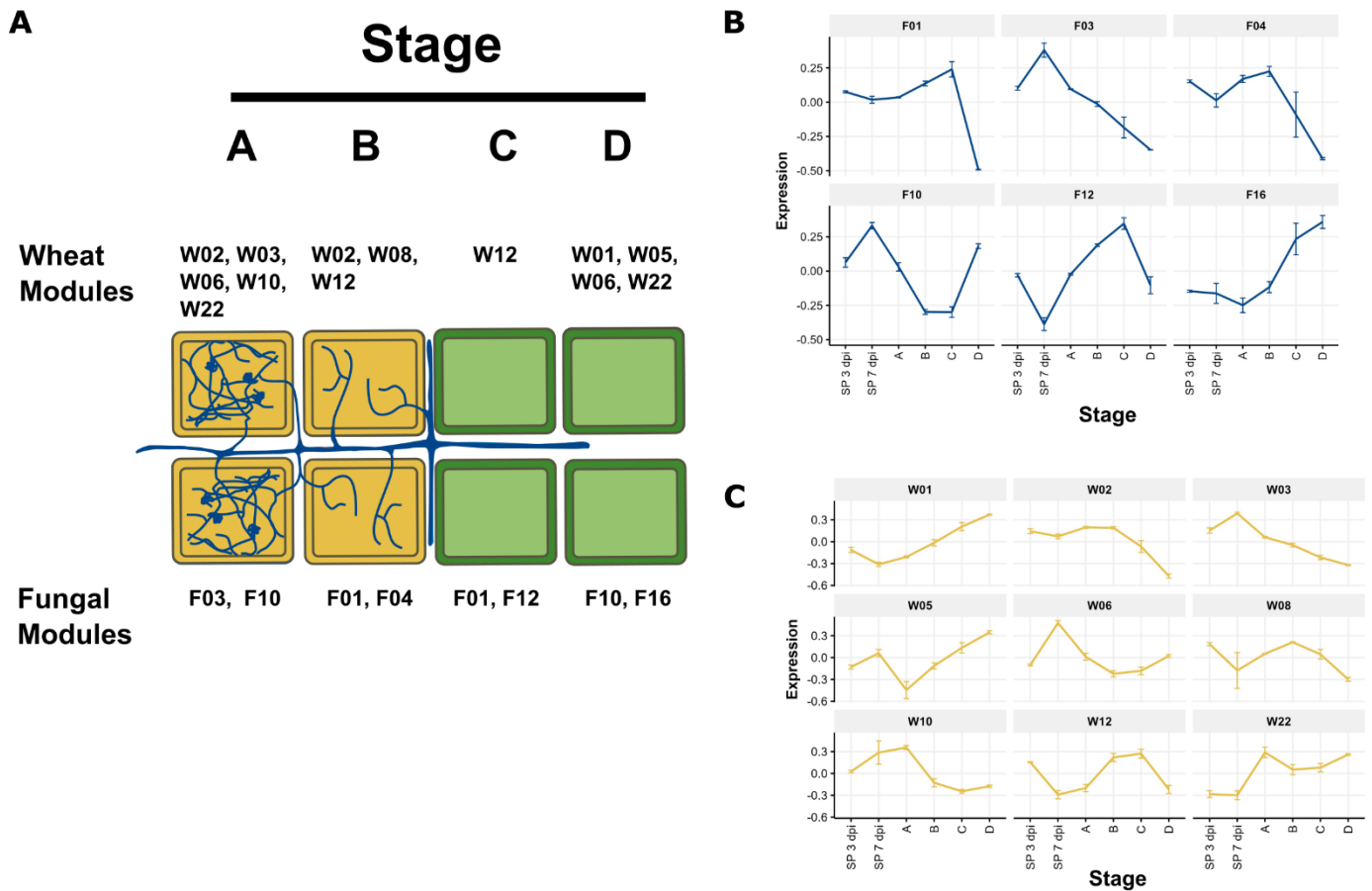
1154 (N = 3). Significance was determined by a one-way ANOVA followed by Tukey HSD

1155 correction. **C.** Normalised fold change expression of selected W12 wheat genes in Mock,

1156 $\Delta Fgtri5$, and WT-recovered RI1-2 tissue sampled at 3 dpi (N = 3). Significance is denoted as

1157 * = $p \leq 0.05$, ** = $p \leq 0.01$, and *** = $p \leq 0.001$. Significance was determined by a one-way

1158 ANOVA followed by Tukey HSD correction.



1159

1160 **Figure 4. Stage-specific expression of modules in the dual co-expression network. A.**

1161 Expression of modules across stages of *F. graminearum* infection. Illustration depicting

1162 symptomatic (yellow) and symptomless (green) stages of infection (A through D) annotated

1163 with specific modules (W or F) from the dual co-expression network that were highly

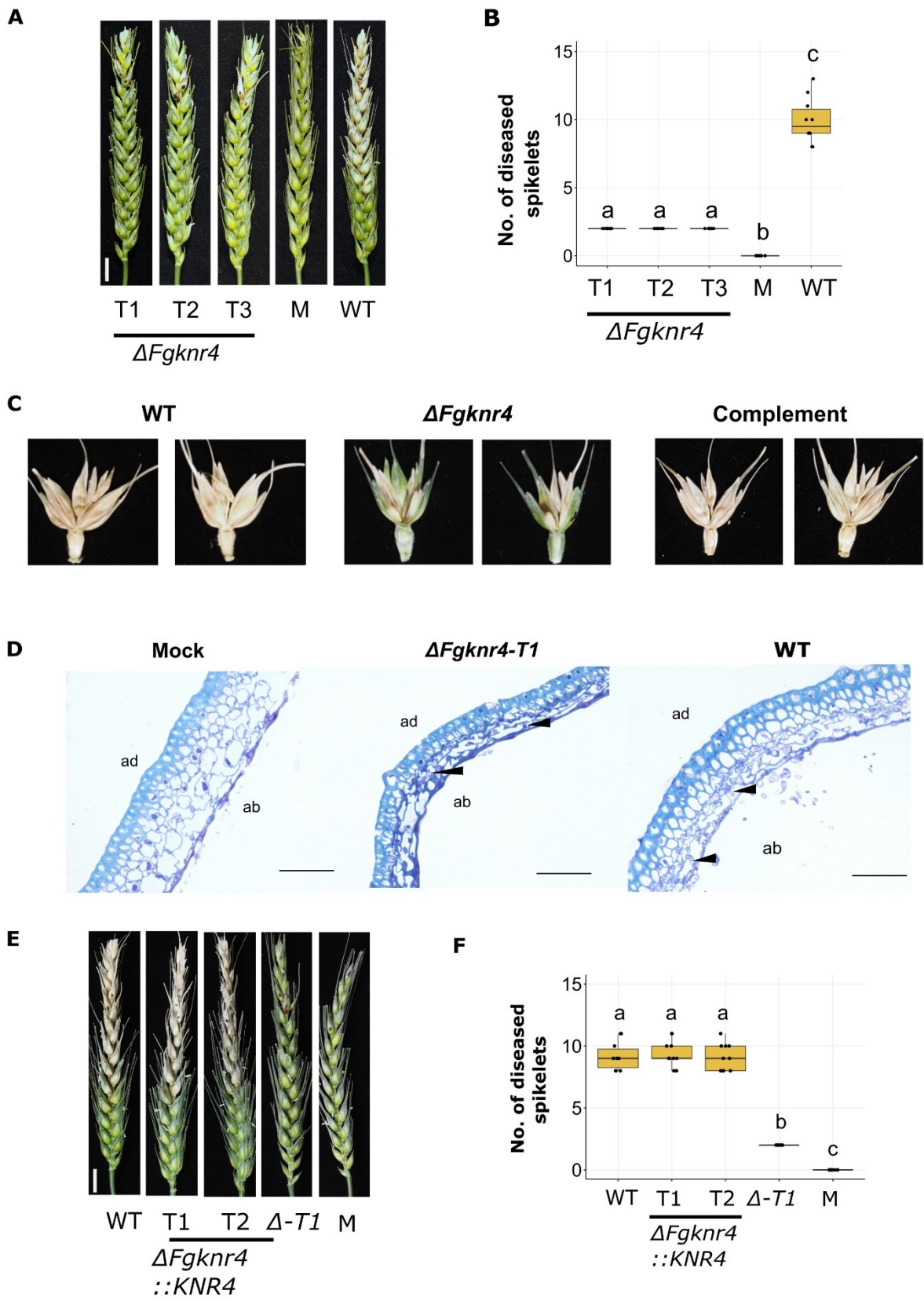
1164 expressed at specific stages. **B. Eigengene summarised expression of fungal modules**

1165 and **C. wheat modules.** Eigengene summarised expression plots illustrating the expression

1166 patterns of genes in wheat modules across different stages of infection as illustrated in panel

1167 A, along with spikelet tissue (SP) at 3 and 7 dpi.

1168



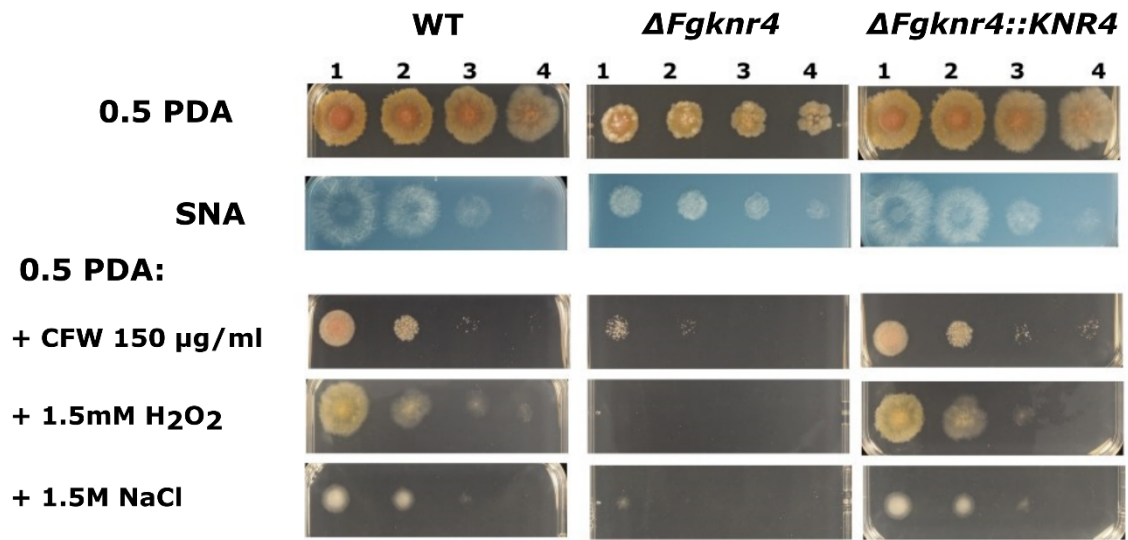
1169

1170

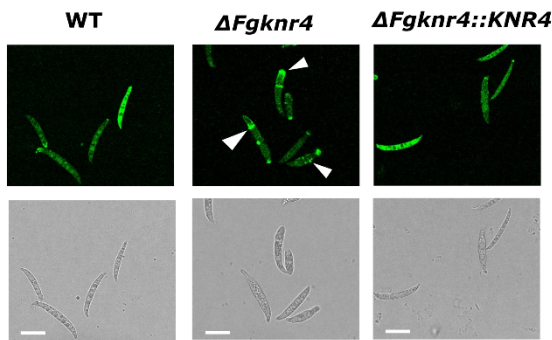
1171 **Figure 5. Decreased virulence observed during *in planta* infection with $\Delta Fgknr4$. A.**
1172 Wheat spike infection assay done on the susceptible cultivar Bobwhite point inoculated with
1173 sterile water only (Mock), wild-type *F. graminearum* conidia, or conidia from three
1174 independent single gene deletion *F. graminearum* mutants lacking *Knr4* ($\Delta Fgknr4$, T1-3).
1175 Images were captured at 15 dpi. Scale bar = 1 cm. **B.** Number of diseased spikelets per
1176 wheat spike at 15 dpi (N = 10). Letters indicate significant differences (ANOVA, TukeyHSD p
1177 < 0.05). **C.** Symptom development on the inoculated spikelets and adjacent rachis tissues at
1178 15 dpi **D.** Ultra-thin 1 μm LR White resin sections stained with 0.1% Toluidine Blue for
1179 visualisation of wheat cell walls (light blue) and fungal hyphae (purple). Black arrows indicate
1180 fungal hyphae. Fungal hyphae typically proliferate in the abaxial cell layer. Ab = abaxial and
1181 ad = adaxial. Scale bar = 50 μm . Tissue harvested at 7 dpi. **E.** Wheat spike infection
1182 complementation assay done on the susceptible cultivar Bobwhite treated with conidia either
1183 from wild-type *F. graminearum*, different complemented transformants ($\Delta Fgknr4::KNR4-T1$
1184 and $T2$), the single gene deletion mutant ($\Delta Fgknr4-T1$), or sterile water (mock). Images were
1185 taken at 15 days post inoculation. **F.** Number of diseased spikelets per wheat spike at 15 dpi
1186 (N = 10). Letters indicate significant differences (ANOVA, TukeyHSD p < 0.05).

1187

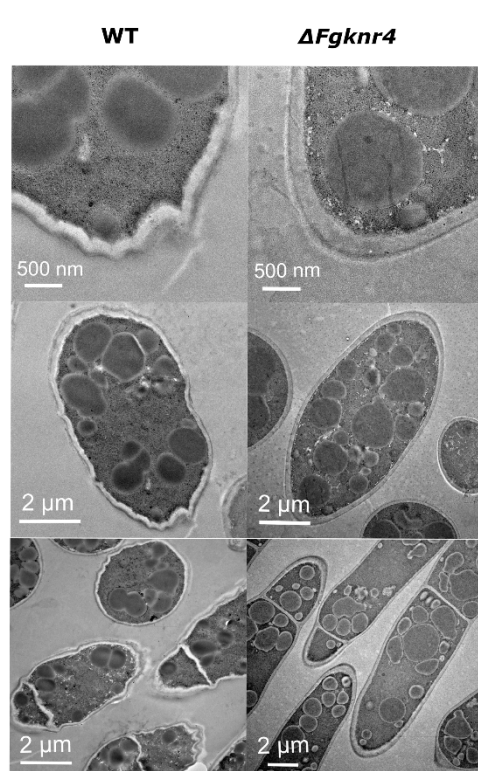
A



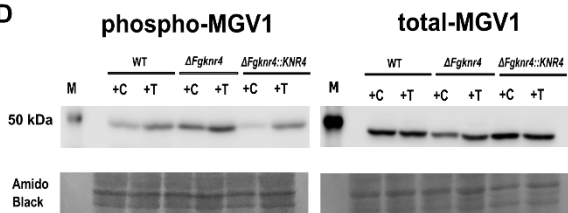
B



C

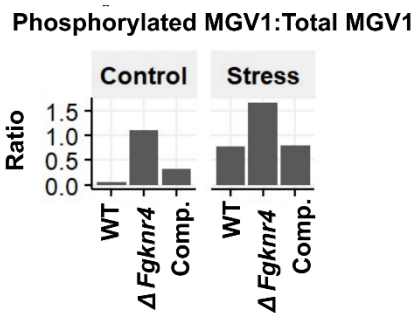


D



Legend: M Marker, C Control (Water), T Treatment (200 $\mu\text{g/ml}$ CFW)

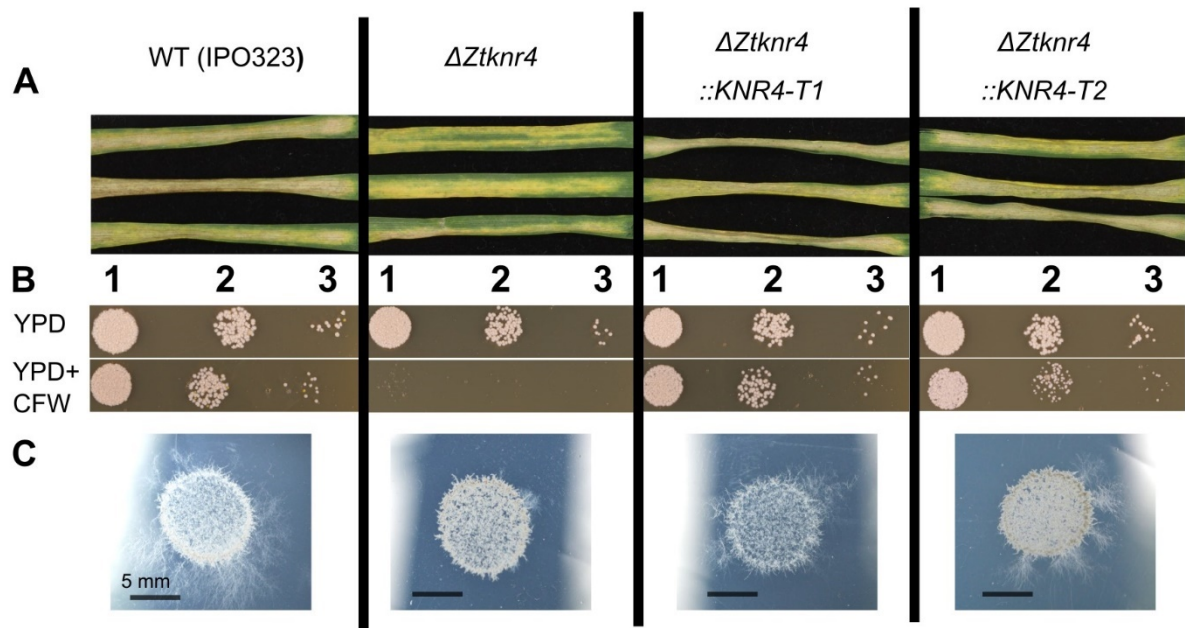
E



1190 **Figure 6. Cell wall stress sensitivity and abnormal cell wall morphology of $\Delta Fgknr4$.** **A.**
1191 Dilution series of wild-type (WT), $\Delta Fgknr4$, and $\Delta Fgknr4::KNR4$ strains on Synthetic Nutrient
1192 Agar (SNA) and half-strength Potato Dextrose Agar (0.5 PDA) with and without the addition
1193 of calcofluor white (CFW), hydrogen peroxide (H_2O_2), and sodium chloride (NaCl). The
1194 dilution series begins at 1: 1×10^6 and continues with 10-fold dilutions (2: 1/10, 3: 1/100, and
1195 4: 1/100). Images taken after 3 days of growth at room temperature. **B.** Abnormal chitin
1196 deposition patterns in $\Delta Fgknr4$ conidia. Chitin-stained in conidia visualised using Wheat
1197 Germ Agglutinin Alexa Fluor™ 488 Conjugate (WGA). Scale bar = 50 μm . **C.** TEM imaging
1198 of wild-type and $\Delta Fgknr4$ conidia, showing differences in cell wall structure **D.** Western blot
1199 of proteins extracted from, $\Delta Fgknr4$ and $\Delta Fgknr4::KNR4$ mycelium incubated with (T) or
1200 without (C) the addition of 200 $\mu g/ml$ Calcofluor White (CFW) for 24 h. Phospho-p44/42
1201 MAPK (Erk1/2) and p44/42 MAPK (Erk1/2) antibodies were used to detect phosphorylated
1202 and total MG1, respectively. Amido black total protein staining was performed to compare
1203 protein loading. **E.** Ratio of phosphorylated MAPK/total MAPK based on quantification of
1204 band intensity.

1205

1207 **Figure 7. Distribution of Knr4 orthologues across eukaryotes reveals exclusive presence in fungi.** A phylogenetic tree depicting the
1208 distribution of *Knr4* orthologues across Eukaryota, with the positions of *F. graminearum* and *Z. tritici* highlighted in red. Different taxonomic
1209 levels are indicated in various colours as specified in the legend, alongside the percent distribution of orthologues between Ascomycota and
1210 Basidiomycota. Evolutionary distances between species or taxa are denoted by an internal scale (range 0 - 3.5) Bootstrapping confidence
1211 values are depicted as pale blue circles, with increasing size corresponding to higher confidence levels.



1212

1213 **Figure 8. Functional characterisation of the *Zymoseptoria tritici* $\Delta Ztknr4$ gene**

1214 **deletion mutant. A.** Detached wheat leaves inoculated with wild-type (WT) *Z. tritici*

1215 (IPO323), $\Delta Ztknr4$ mutant strain, and two complemented strains ($\Delta Ztknr4::KNR4-T1$ and

1216 $T2$). Images taken at 20 dpi. **B.** WT *Z. tritici*, the $\Delta Ztknr4$ mutant and two complemented

1217 strains ($\Delta Ztknr4::KNR4-T1$ and $T2$) spot inoculated onto YPD agar with (bottom) and without

1218 (top) calcofluor white (CFW). Dilution series begins at 1: 1×10^5 and continues with 10-fold

1219 dilutions (2: 1/10 and 3: 1/100). Images taken after 3 days of growth at room temperature

1220 (RT). **C.** WT *Z. tritici*, the $\Delta Ztknr4$ mutant and two complemented strains ($\Delta Ztknr4::KNR4-T1$

1221 and $T2$) spot inoculated onto 1% Tap Water Agar (TWA). Images taken after 10 days of

1222 growth at room temperature (RT).

A

Module	Module Size	GO MF/BP Summary	GO CC Summary	Trait Ontology (TO)
25	83	DNA integration	Cell periphery	ethylene sensitivity
24	96	Isopentenyl diphosphate biosynthesis	-	callus induction
23	153	Protein modification	-	other miscellaneous trait
22	183	-	-	other miscellaneous trait
21	199	-	-	total root number
20	235	DNA packaging	Nucleosome	cytoplasmic male sterility
19	254	Lipid biosynthesis and proteasome activity	Lipid droplet	cytoplasmic male sterility
18	287	Ubiquitination and protein catabolism	Proteasome complex	auxin sensitivity
17	316	Diterpenoid biosynthesis	Extracellular region	cytoplasmic male sterility
16	332	Protein phosphorylation and kinase activity	Integral component of membrane	disease resistance
15	334	Fatty acid metabolism and synthesis	-	plant height
14	374	Translation	Cytosolic ribosome	stem elongation
13	379	Structural constituent of ribosome	Cytosolic ribosome	leaf senescence trait
12	451	Detoxification and response to toxic substance	-	sheath blight disease resistance
11	501	Glycolysis	-	self-incompatibility
10	695	Protein localisation and autophagy	Protein-containing complex	male sterility
9	765	Protein phosphorylation and kinase activity	Integral component of membrane	germination rate
8	818	Protein phosphorylation and defense response	Integral component of membrane	disease resistance
7	1544	Response to water and water channel activity	Chloroplast	cold tolerance
6	1552	Protein catabolism and autophagy	Proteasome complex	days to flowering trait
5	1802	Vesicle transport and hydrolase activity	Vesicle	disease resistance
4	2344	Gene expression	Ribonucleoprotein complex	disease resistance
3	3125	Proteolysis and autophagy	Peroxisome	disease resistance
2	7573	Glutathione metabolism and response to biotic stimuli	Extracellular region	disease resistance
1	23063	RNA modification and defense response	Chloroplast	harvest index

B

Module	Module size	Phenotype				GO MF/BP Summary	GO CC Summary	Gene set enrichment				
		LOP	RV	L	U			TRI Genes	BMCs	Protein Kinases	Transcription Factors	Predicted Effectors
18	60	0	0	0	3	-	-					
17	62	0	0	0	3	-	-					
16	74	0	4	0	2	-	-					
15	75	0	0	0	2	-	-					
14	79	0	2	1	3	-	-					
13	121	0	2	0	6	-	-					
12	124	3	11	0	6	Terpenoid metabolic process	Extracellular region					
11	253	0	6	1	15	-	-					
10	275	0	11	0	14	-	-					
9	353	1	13	5	25	-	-					
8	406	0	10	1	9	-	-					
7	442	0	0	0	1	Translation	Cytoplasm					
6	607	0	9	3	35	-	-					
5	647	2	43	13	26	Metabolic processes	Cytoplasm					
4	1217	1	9	6	88	Transcription factor activity	Ribosome					
3	1278	0	6	1	77	Oxidoreductase activity	Membrane					
2	1487	4	66	12	88	Cellular Organisation	Membrane					
1	2629	4	65	16	184	Transcription factor activity	Nucleus					

1223

1224 **Figure 2 – figure supplement 1. Network Summary. A.** Summary of all modules in the

1225 wheat network, including module size (number of genes), Gene Ontology (GO) and Trait

1226 Ontology (TO) enrichment summaries. **B.** Summary of all modules in the fungal network,

1227 including modules size, Gene Ontology (GO) enrichment summaries and Gene Set

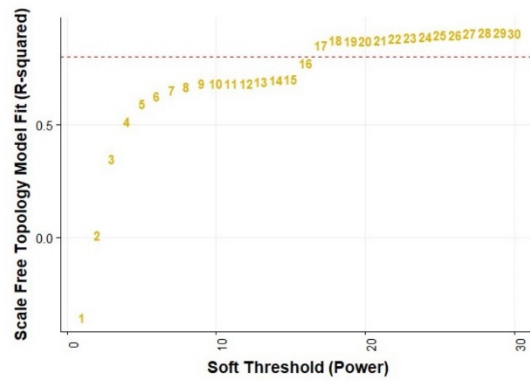
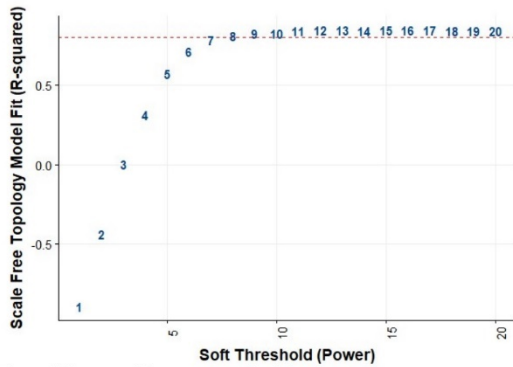
1228 Enrichment Analysis (GSEA). The number of genes with different phenotypes in PHI-base
1229 are depicted, with LOP, RV, L and U denoting different PHI-base phenotypes (LOP = Loss of
1230 pathogenicity; RV = Reduced virulence; L = Lethal; U = Unaffected pathogenicity) (**Urban et**
1231 **al., 2022**).

1232

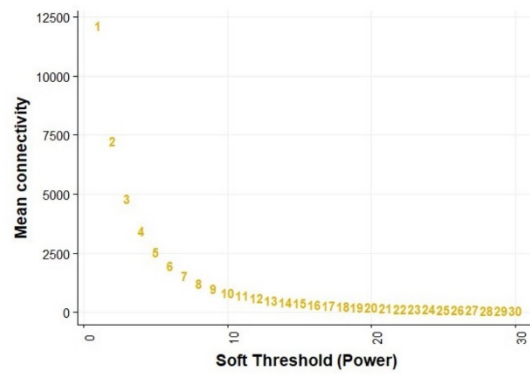
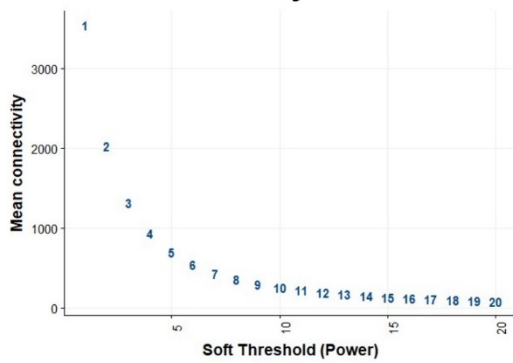
Fungal

Wheat

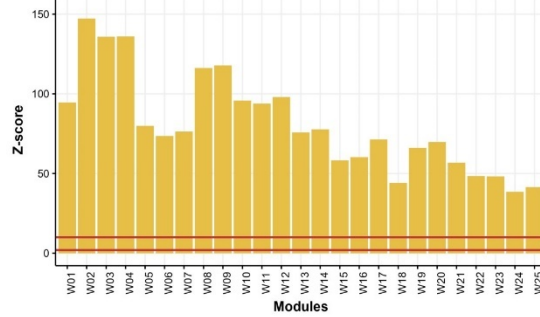
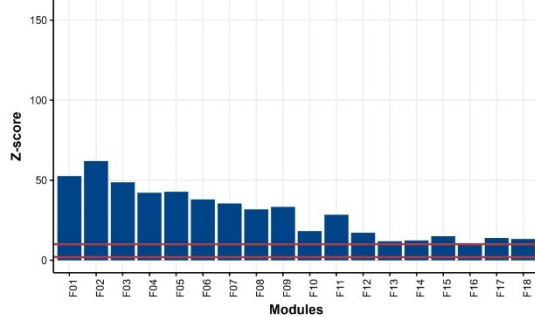
A. Scale Free Model Fit



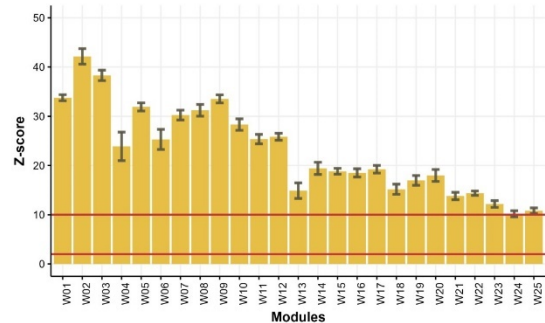
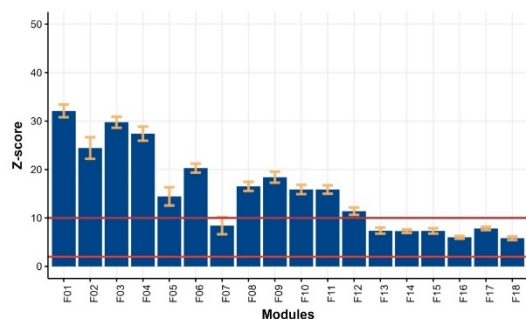
B. Mean Connectivity



C. Module Quality



D. Module Preservation



1233

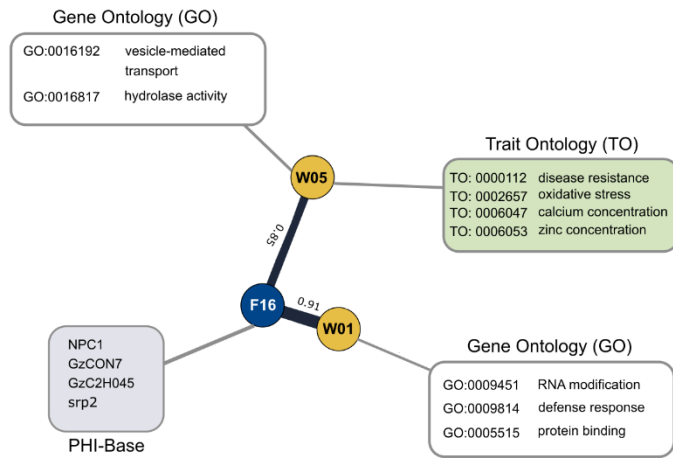
1234 **Figure 2 – figure supplement 2. Network statistics. A.** Strength of correlation of network

1235 model (R-squared value) to scale free model at different soft thresholding powers. Dotted

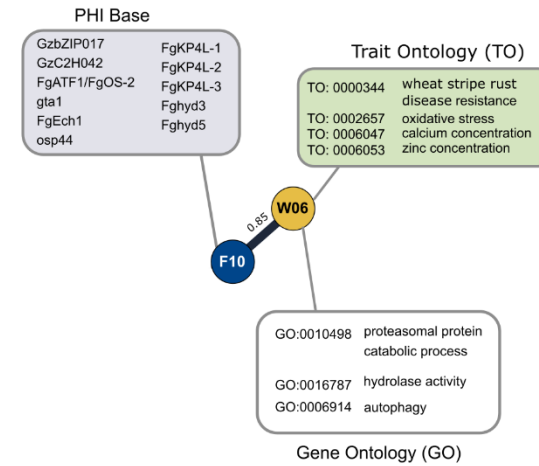
1236 red line is at an R-squared value of 0.80, the threshold needed for generating a WGCNA
1237 network. **B.** Mean connectivity of genes in each network at different soft thresholding
1238 powers. A low mean connectivity is desired to meet the scale free network criteria. **C.**
1239 Module quality across all modules as determined by a Z-score calculation. Solid red lines at
1240 minimum quality ($Z = 2$) and high quality scores ($Z = 10$). **D.** Module preservation as
1241 determined by Z-score calculation against 50 random test networks. Solid red lines at
1242 minimum preservation ($Z = 2$) and high preservation scores ($Z = 10$).

1243

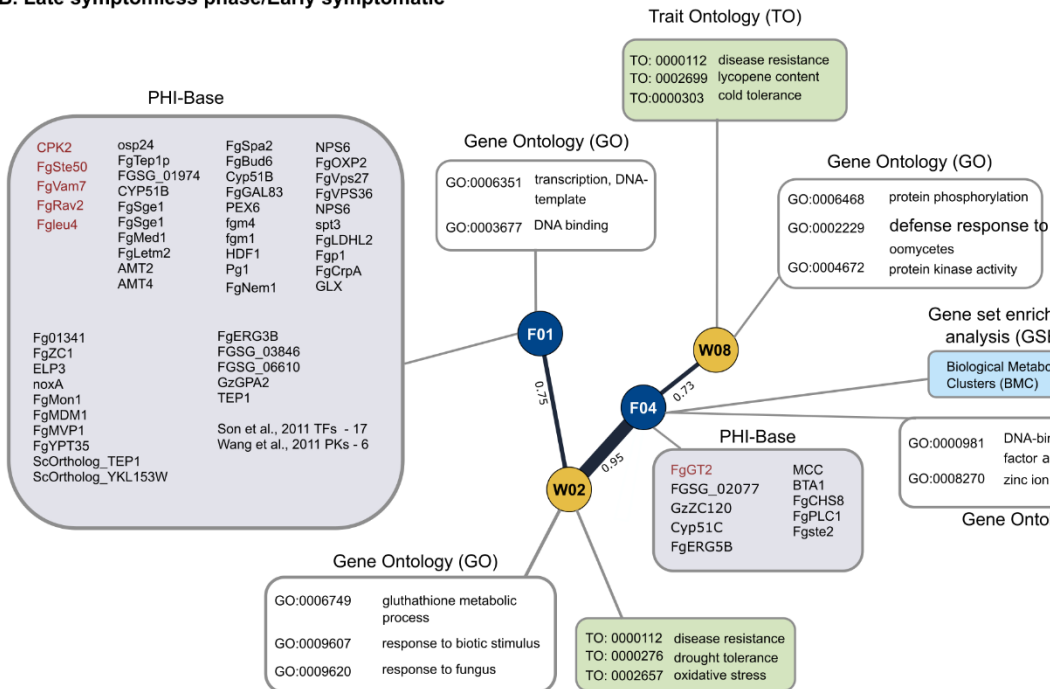
A. Early symptomless phase



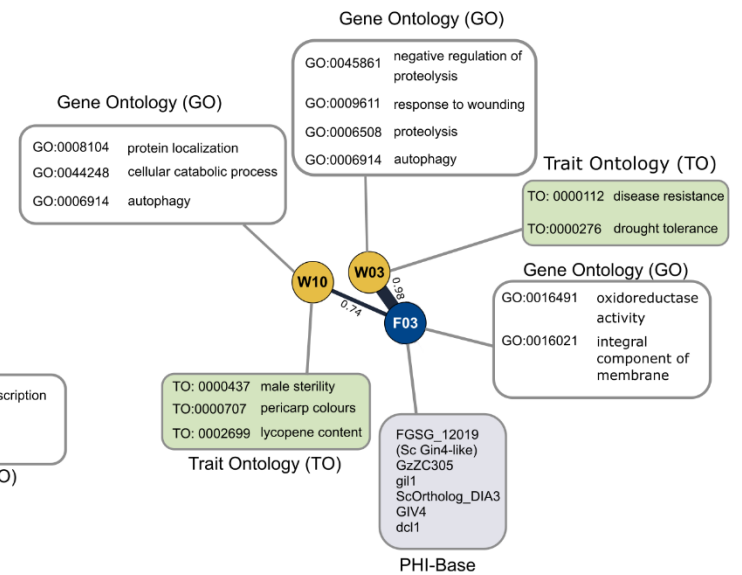
B. Early symptomless and late symptomatic



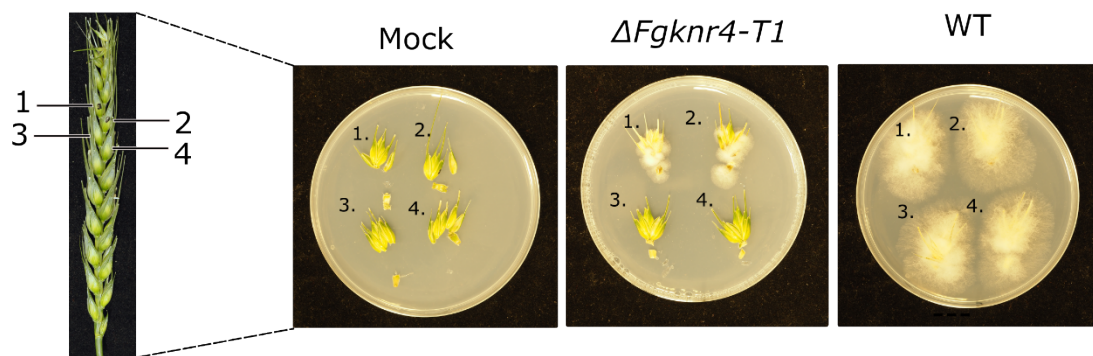
B. Late symptomless phase/Early symptomatic



C. Late symptomatic phase



1245 **Figure 4 – figure supplement 1. Annotation of stage-specific modules.** Fungal modules (F) and wheat modules (W) depicted with
1246 significant enrichment annotations. Fungal modules are additionally annotated with known phenotypes from PHI-base. Genes listed in red in
1247 the PHI-base annotation (grey box) exhibit a loss of pathogenicity phenotype when deleted, while the remaining genes display a reduced
1248 virulence phenotype when deleted. Plots are separated by modules with highest expression in a given stage of infection, namely **A. Early**
1249 **symptomless, B. Early symptomless and late symptomatic, C. Late symptomless/Early symptomatic, and D. Late symptomatic.**
1250



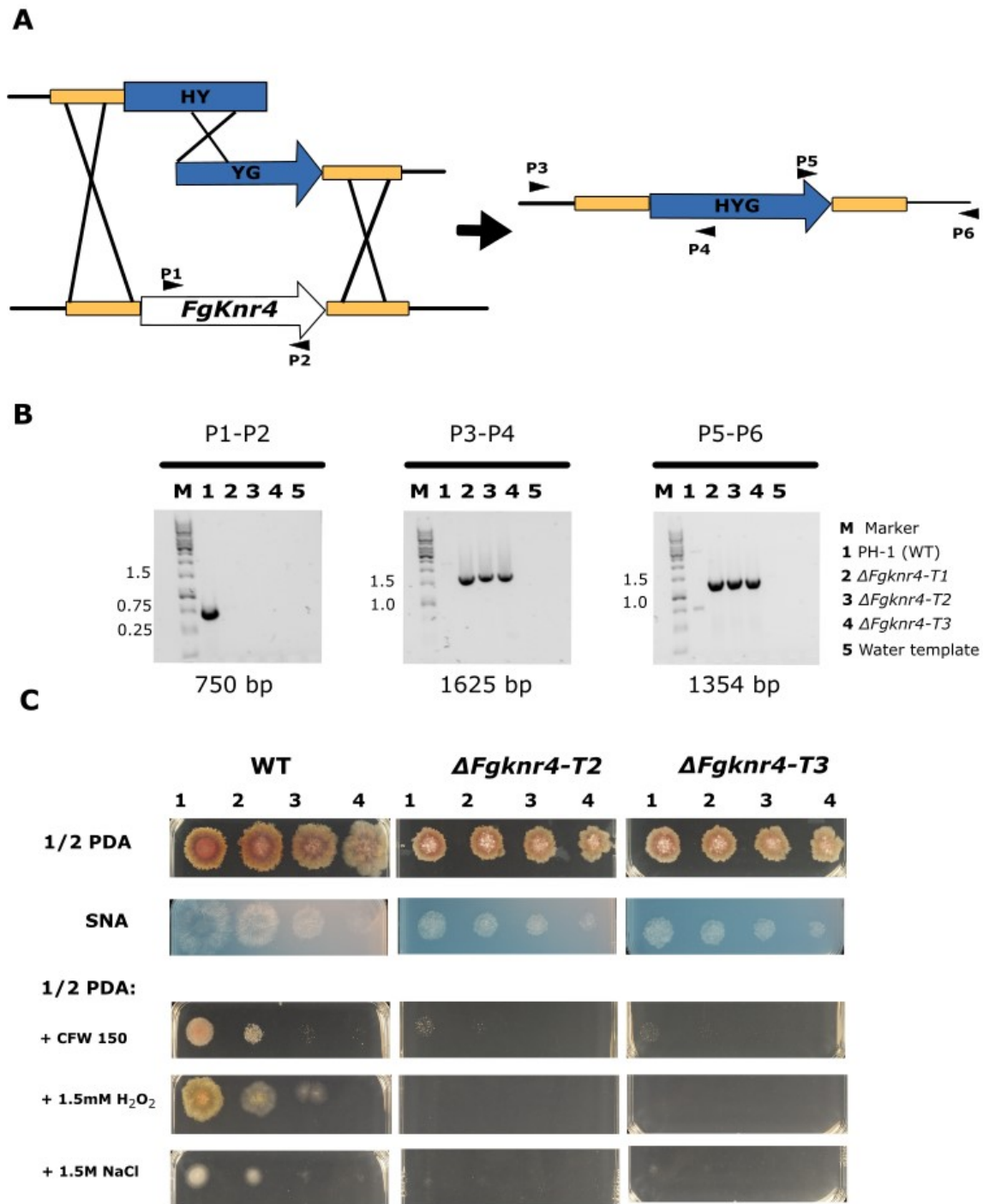
1251

1252 **Figure 5 – supplement 1. Surface sterilisation of dissected wheat floral tissue.**

1253 Dissection at 15 dpi of wheat spikes followed by separation of infected wheat spikelet and

1254 rachis tissues and subsequent plating onto synthetic nutrient agar (SNA) separated at 15

1255 dpi. Plate images taken 3 days later.



1256

1257 **Figure 6 – figure supplement 1. *FgKnr4* single gene deletion strategy and**

1258 **characterisation of additional transformants. A. Schematic for the hygromycin split**

1259 **marker deletion strategy including diagnostic primer locations (P1-6). B. Diagnostic PCR**

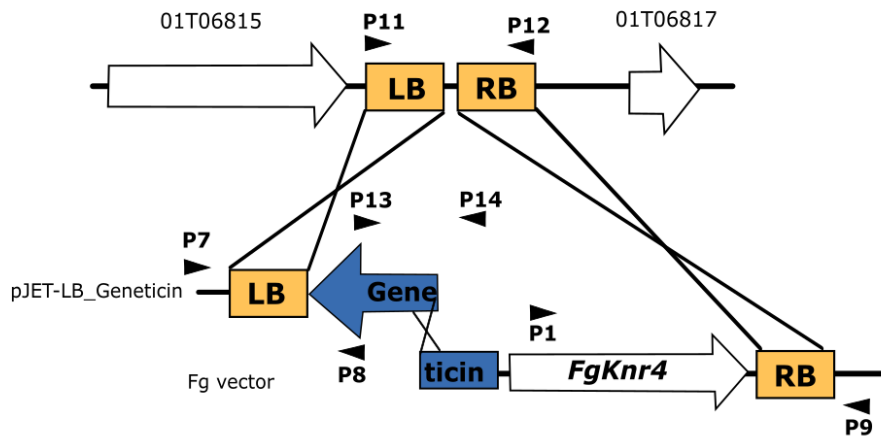
1260 **with primer sets depicted in panel A. PCR samples were separated on 7.5 % agarose gel**

1261 with a 1 kb DNA ladder. The expected amplicon size is written below the corresponding gel
1262 image. **C.** Dilution series of wild-type (WT) and additional $\Delta Fgknr4$ transformants (*T2* and
1263 *T3*) on Synthetic Nutrient Agar (SNA) and half-strength Potato Dextrose Agar (0.5 PDA) with
1264 and without the addition of single stresses. The dilution series begins at 1: 1×10^6 and
1265 continues with 10-fold dilutions (2: 1/10, 3: 1/100, and 4: 1/100). Images taken after 3 days.

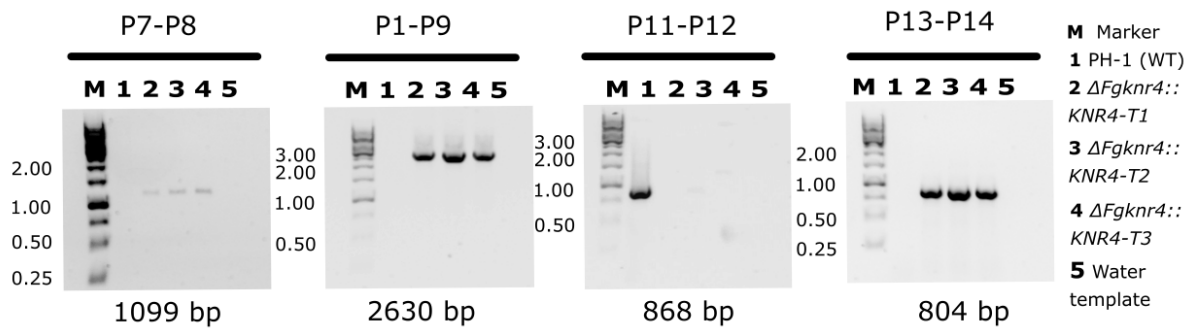
1266

1267

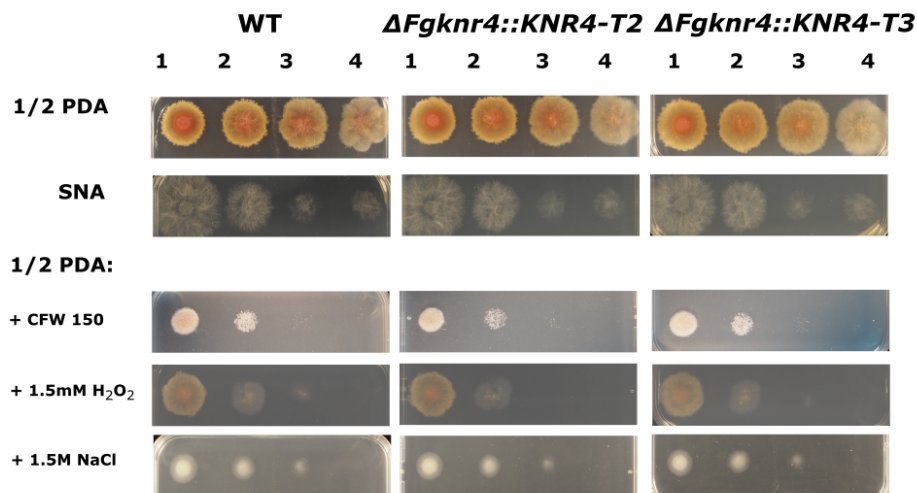
A



B



C



1268

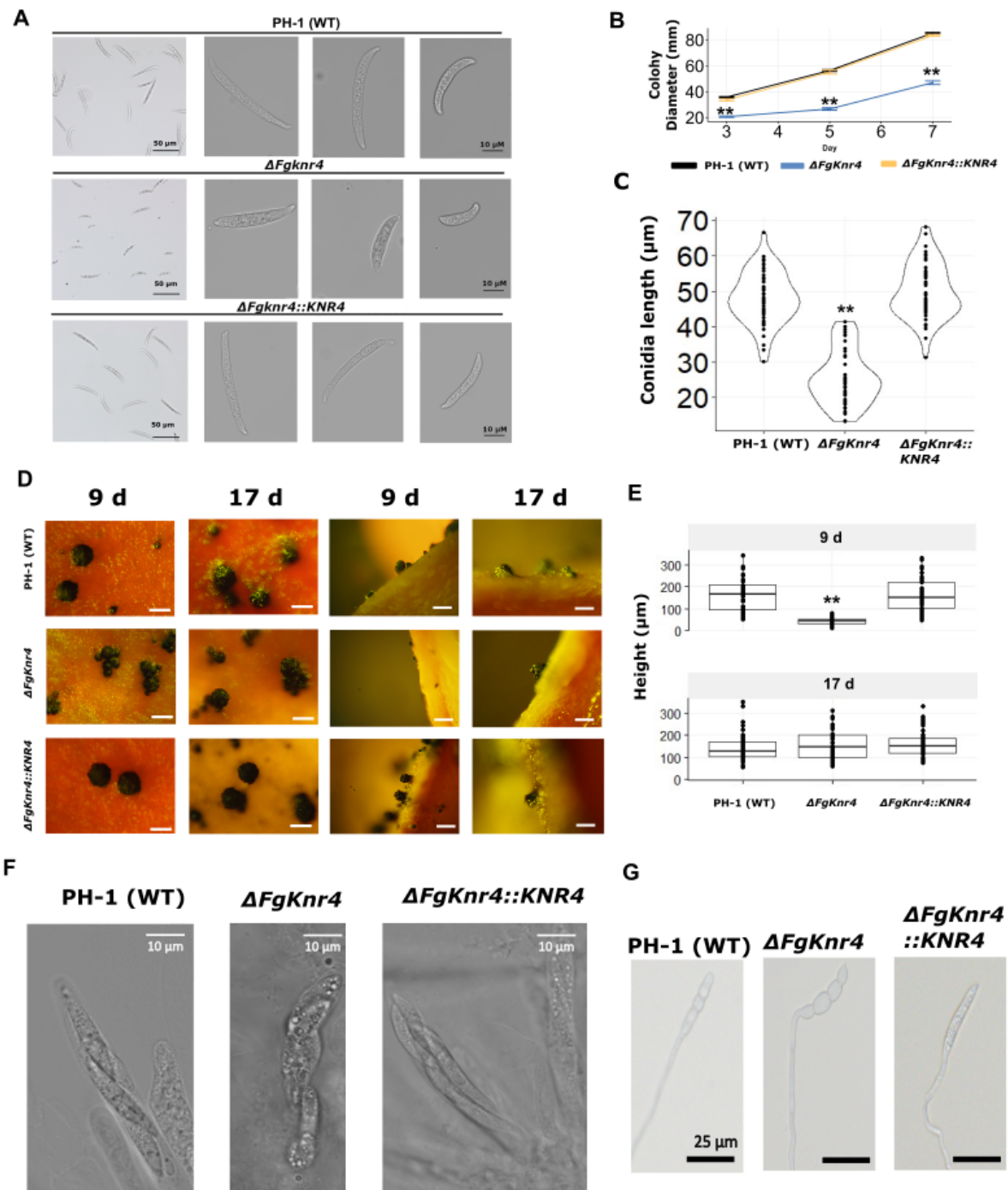
1269 **Figure 6 – figure supplement 2. $\Delta Fgknr4-T1$ complementation strategy and**

1270 **characterisation of additional transformants. A. Schematic of gene complementation into**

1271 **the *Fg* transformation locus (Darino et al. 2024), including diagnostic primer locations. B.**

1272 Diagnostic PCR with primer sets depicted in panel A. PCR samples were separated on 7.5
1273 % agarose gel with a 1 kb DNA ladder. Expected amplicon size is written below the
1274 corresponding gel image. **C.** Dilution series of wild-type (WT) and additional $\Delta Fgknr4::KNR4$
1275 transformants (*T2* and *T3*) on Synthetic Nutrient Agar (SNA) and half-strength Potato
1276 Dextrose Agar (0.5 PDA) with and without the addition of single stresses. The dilution series
1277 begins at 1: 1×10^6 and continues with 10-fold dilutions (2: 1/10, 3: 1/100, and 4: 1/100).
1278 Image taken after 3 days.

1279



1280

1281

Figure 6 – figure supplement 3. Characterisation of growth rate, conidial size and

1282

ascospore production in $\Delta Fgknr4$ and complemented strains. **A.** Decreased conidial size

1283

observed in $\Delta Fgknr4$. Single conidial images to represent long, middle length, and short

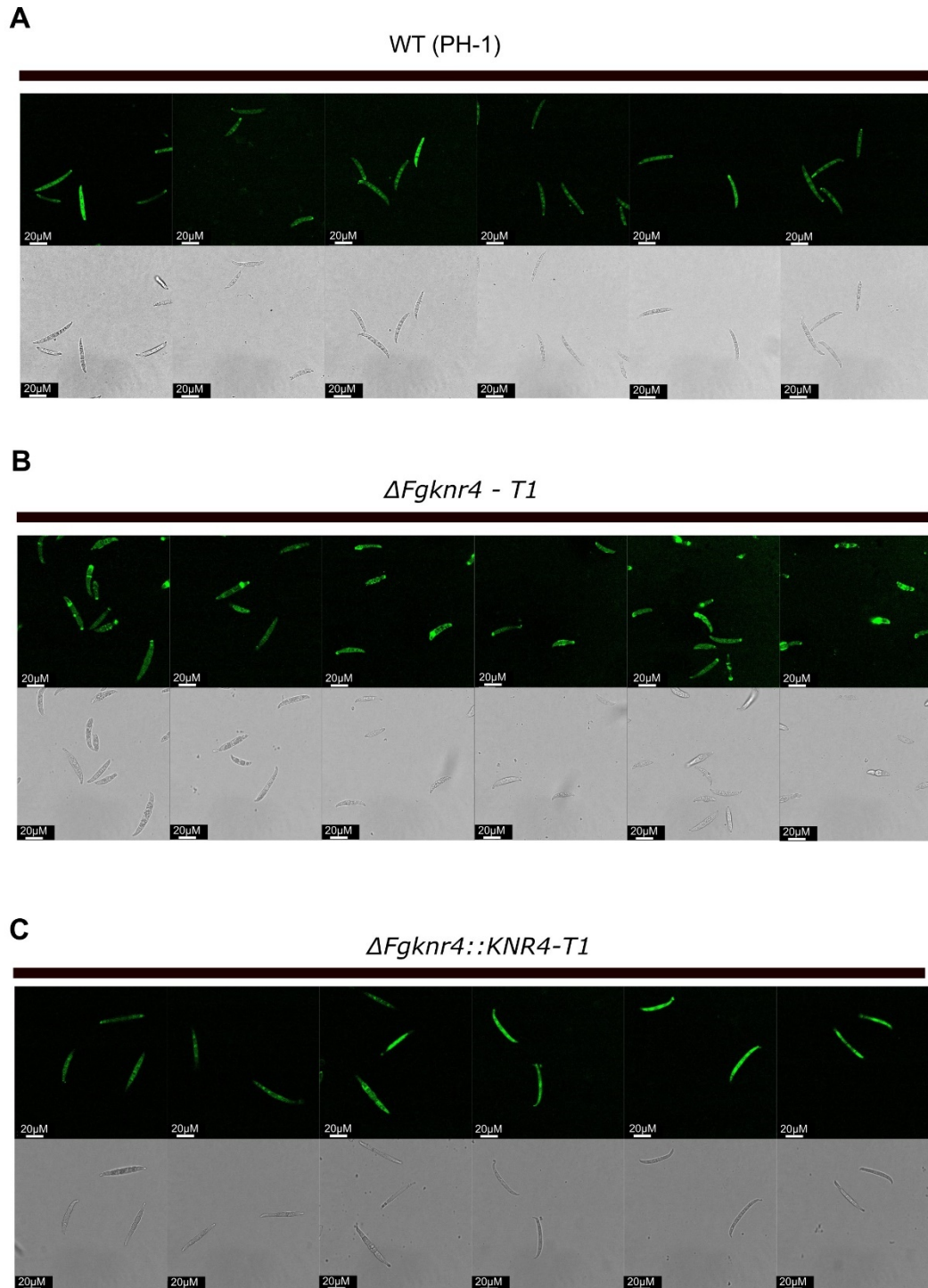
1284

conidia across strains. **B.** Mean colony diameter of wild-type (WT), $\Delta Fgknr4$, and

1285

$\Delta Fgknr4::KNR4$ grown on Potato Dextrose Agar (PDA) (N = 5). **C.** Distribution of conidial

1286 length from N = 50 spores for WT, *ΔFgknr4*, and *ΔFgknr4::KNR4* strains. **D.** Representative
1287 perithecia images taken after perithecia induction in carrot agar medium using WT, *ΔFgknr4*,
1288 and *ΔFgknr4::KNR4* strains. Images taken from above (left panels) and from agar sections
1289 placed on slides (right panels) on day 9 and day 17. Scale bar = 500 μm. **E.** Mean perithecia
1290 height of WT, *ΔFgknr4*, and *ΔFgknr4::KNR4* after 9 and 17 days (N = 40). **F.** Ascospores in
1291 intact ascus produced by wild-type (WT), *ΔFgknr4* or *ΔFgknr4::KNR4* strains. Scale bar = 10
1292 μm. **G.** Ascospores obtained from squashed perithecia of wild-type (WT), *ΔFgknr4* or
1293 *ΔFgknr4::KNR4* strains are viable and form germ tubes. Scale bar = 25 μm. Significance is
1294 denoted as ** = $p \leq 0.01$. Significance was determined by a one-way ANOVA followed by
1295 Tukey HSD correction.



1296

1297 **Figure 6 – figure supplement 4. Additional fluorescent microscopy images of irregular**

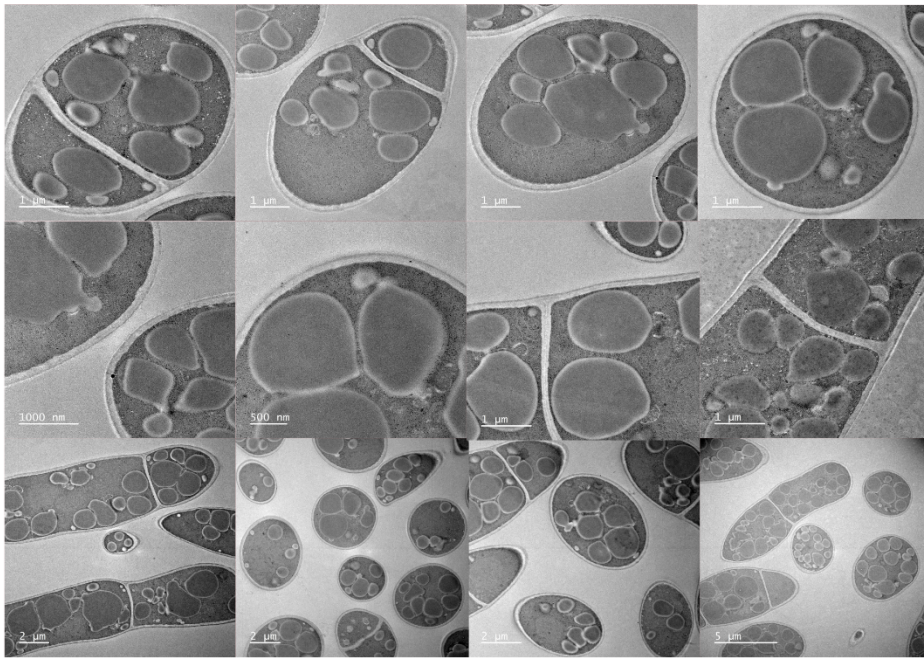
1298 **chitin distribution in $\Delta Fgknr4$ conidia.** Visualisation of chitin-stained conidia with Wheat

1299 Germ Agglutinin Alexa Fluor™ 488 Conjugate (WGA) in wild-type (WT) **(A)**, $\Delta Fgknr4$ **(B)** and

1300 $\Delta Fgknr4::KNR4$ **(C)**.

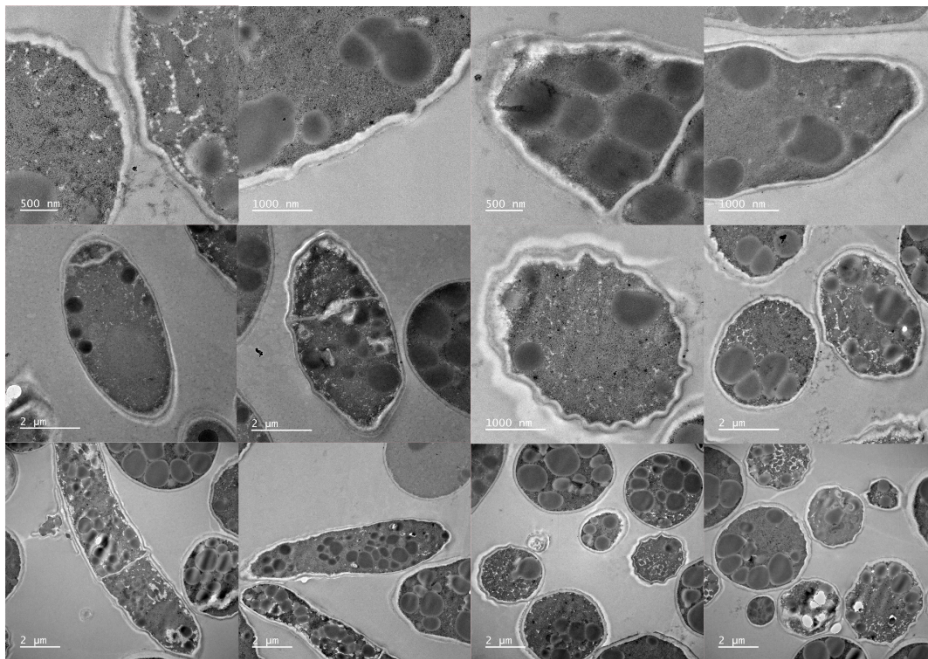
A

WT (PH-1)



B

$\Delta Fgknr4$ - T1

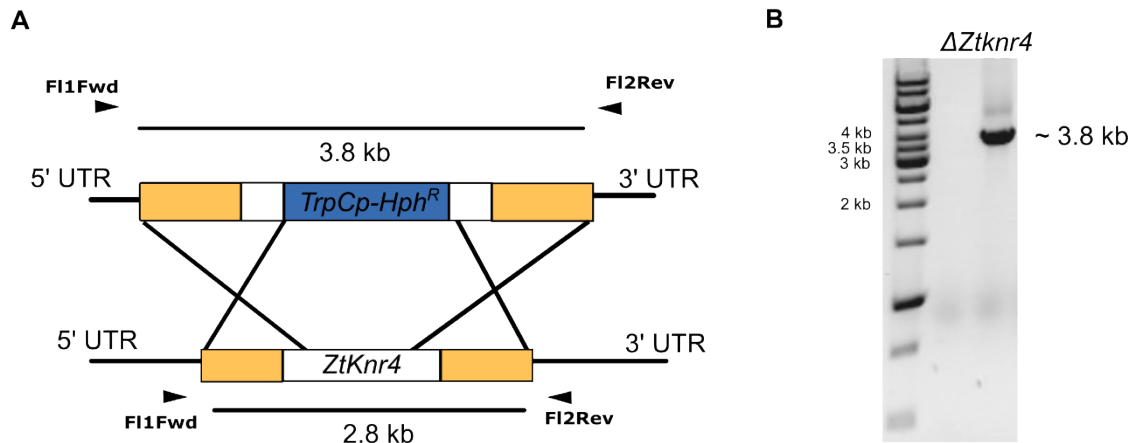


1301

1302 **Figure 6 – figure supplement 5. Additional TEM images of abnormal cell wall**

1303 **morphology in $\Delta Fgknr4$ conidia. TEM imaging of wild-type (A) and $\Delta Fgknr4$ (B) conidia,**

1304 **showing differences in cell wall structure and different magnifications.**



1305

1306 **Figure 8 – figure supplement 1.** $\Delta Ztknr4$ diagnostic PCR and disruption deletion strategy.

1307 **A.** Hygromycin (Hph^R) replacement cassette inserts at $ZtKnr4$ locus through homologous
 1308 recombination via homologous flanks (yellow and white). **B.** Diagnostic PCR demonstrating
 1309 presence of large insertion fragment in $\Delta Ztknr4$ transformant using FI1Fwd and FI2Rev
 1310 primers.

1311 **Supplementary File S1. Network module sizes and gene module assignments.**

1312 Spreadsheet containing sizes of all modules in fungal and wheat networks. 'Fungal module
1313 assignments' and 'Wheat module assignments' tabs contain a column with all fungal IDs
1314 (RRES v.5 PH-1) or wheat IDs (Column A = IWGSC RefSeq v2.1; Column B = IWGSC
1315 RefSeq v1.1) with an adjacent column denoting which module they are clustered in.

1316 **Supplementary File S2. *F. graminearum* genes with known phenotypes with the PHI-base**
1317 **database (www.PHI-base.org) in each fungal module. Table provides RRES v5 gene ID,**
1318 **PHI identifier ID from PHI-base, Uniprot protein ID, gene function, mutant phenotype, author**
1319 **reference, and year published.**

1320 **Supplementary File S3. Primer list.** Primers used to generate mutant and complemented
1321 strains.

1322

1323

1324 **Table S1. Candidate gene selection in fungal module F16.** Table provides details on the 15 candidates within module F16 with the highest
 1325 module membership (MM) and reason for exclusion from further functional characterisation analysis. This table includes the MM score and
 1326 associated *p*-values (p.MM), as well as correlation strength to corresponding wheat modules (Cor) and *p*-values (p.Cor).

ID	COR.W05	P.COR.W0	COR.W01	P.COR.W01	MM.F16	P.MM.F16	INTERPRO DESCRIPTION	REASON FOR EXCLUSION
		5						
FGRAMPH1_01T20453	0.79	0.00	0.93	0.00	0.95	0.00	N/A	Unknown domain
FGRAMPH1_01T06173	0.88	0.00	0.77	0.00	0.94	0.00	domain of unknown function DUF2405;	Unknown domain
FGRAMPH1_01T22959	0.69	0.00	0.94	0.00	0.93	0.00	RNA recognition motif domain;U1 small nuclear ribonucleoprotein of 70kDa N-terminal;snRNP70, RNA recognition motif;RNA-binding domain superfamily;U1 small nuclear ribonucleoprotein 70kDa	75 genes with this domain in <i>F. graminearum</i> proteome

FGRAMPH1_01T10513	0.73	0.00	0.76	0.00	0.91	0.00	Helicase, C-terminal;DEAD/DEAH box helicase domain;Helicase superfamily 1/2, ATP-binding domain;P-loop containing nucleoside triphosphate hydrolase	26 ancient paralogues on Ensembl (2022)
FGRAMPH1_01T00861	0.86	0.00	0.76	0.00	0.91	0.00	BRCT domain;AAA+ ATPase domain;ATPase, AAA-type, core;DNA polymerase III, clamp loader complex, gamma/delta/delta subunit, C-terminal;Replication factor C subunit 1;DNA replication factor RFC1, C-terminal;P-loop containing nucleoside triphosphate hydrolase;BRCT domain superfamily	2 ancient paralogues on Ensembl (2022)
FGRAMPH1_01T00671	0.69	0.00	0.80	0.00	0.91	0.00	PAP/25A-associated;Nucleotidyltransferase superfamily	1 ancient paralogue on Ensembl (2022)

FGRAMPH1_01T00977	0.83	0.00	0.85	0.00	0.90	0.00	Endoplasmic reticulum vesicle transporter, C-terminal;Endoplasmic reticulum vesicle transporter, N-terminal	1 ancient paralogue on Ensembl (2022)
FGRAMPH1_01T18141	0.72	0.00	0.83	0.00	0.90	0.00	CDC48, N-terminal subdomain;AAA+ ATPase domain;ATPase, AAA-type, core;ATPase, AAA-type, conserved site;CDC48, domain 2;Aspartate decarboxylase-like domain superfamily;Vps4 oligomerisation, C-terminal;P-loop containing nucleoside triphosphate hydrolase;CDC48 domain 2-like superfamily;AAA ATPase, AAA+ lid domain	15 ancient paralogues on Ensembl(2022)

FGRAMPH1_01T22333	0.83	0.00	0.75	0.00	0.90	0.00	AMP-dependent synthetase/ligase;Phosphopantetheine binding ACP domain;Trimeric LpxA-like superfamily;Polyketide synthase, phosphopantetheine-binding domain;ACP-like superfamily	BLAST hit in <i>F. graminearum</i> PH-1 genome (E = 4.5e-063)
FGRAMPH1_01T27545	0.71	0.00	0.88	0.00	0.90	0.00	Sterol-sensing domain;Protein patched/dispatched;Niemann-Pick C1, N-terminal	Previously studied. Reduced virulence phenotype (Breakspear et al. 2011)
FGRAMPH1_01T23707	0.82	0.00	0.74	0.00	0.90	0.00	Knr4/Smi1 family;Knr4/Smi1-like domain	
FGRAMPH1_01T27219	0.66	0.00	0.93	0.00	0.89	0.00	N/A	Unknown domain

FGRAMPH1_01T02111	0.81	0.00	0.85	0.00	0.89	0.00	DNA-directed RNA polymerase, subunit 2, hybrid-binding domain;RNA polymerase, beta subunit, conserved site;RNA polymerase Rpb2, domain 7;RNA polymerase Rpb2, domain 2;RNA polymerase, beta subunit, protrusion;RNA polymerase Rpb2, domain 3;RNA polymerase Rpb2, domain 4;RNA polymerase Rpb2, domain 5;DNA-directed RNA polymerase, subunit 2	2 ancient paralogues on Ensembl (2022)
FGRAMPH1_01T04893	0.75	0.00	0.69	0.00	0.88	0.00	SNF2-related, N-terminal domain;Helicase, C-terminal;Helicase superfamily 1/2, ATP-binding domain;DBINO domain;P-loop containing nucleoside triphosphate hydrolase	26 ancient paralogues on Ensembl (2022)
FGRAMPH1_01T07953	0.84	0.00	0.75	0.00	0.88	0.00	Folylpolyglutamate synthetase;Mur-like, catalytic domain	2 paralogues on Ensembl (2022)

superfamily;Mur ligase, C-terminal

domain superfamily

